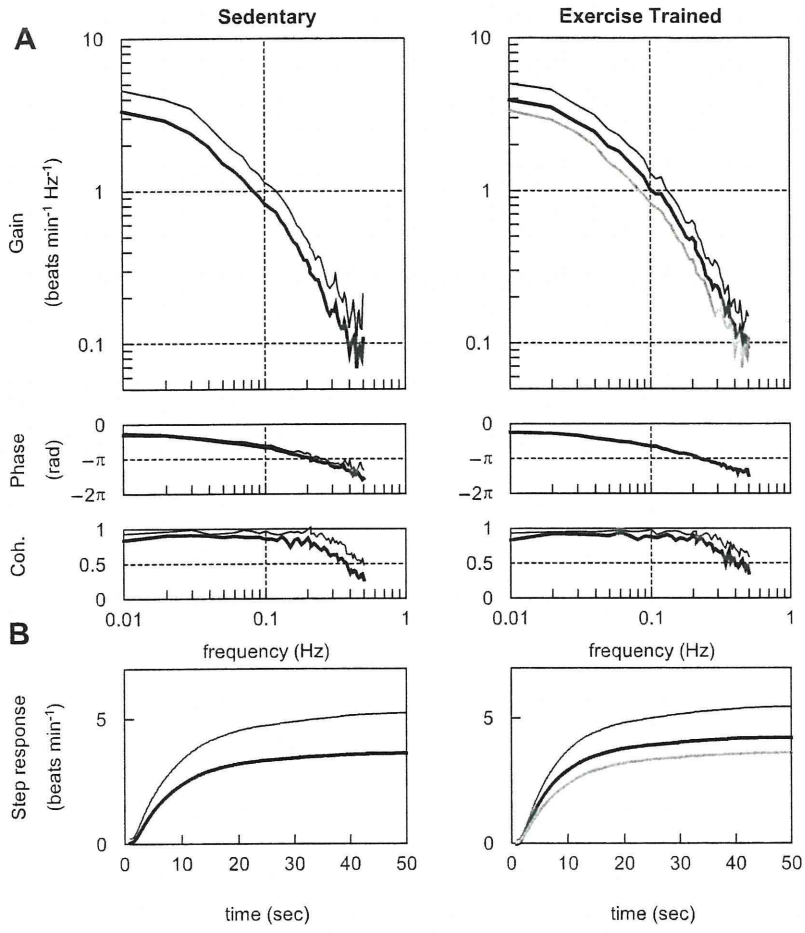

Fig. 2. *A*: transfer function from sympathetic stimulation to the HR response obtained in sedentary and exercised-trained rats. Gains (*top*), phase shifts (*middle*), and coherence (Coh.) functions (*bottom*) are presented. *B*: calculated step response to 1-Hz tonic sympathetic stimulation. Thick lines represent the mean, whereas thin lines indicate ± SD values. The gray solid curves in the gain and step response panels (*right*) duplicates the means (*left*).

pathetic tonus, which can decrease the gain of the vagal transfer function (17).

It has been documented that the intensity of exercise as well as the duration of exercise training are related to the autonomic adaptation to exercise training (28). These factors have been shown to be largely variable among different studies. A well-controlled experimental setup is needed to clarify these issues.

Dynamic Gain Values of Sympathetic and Vagal Transfer Functions Corresponding to HRV Frequency Bands

HRV is considered to reflect autonomic tone (19). The VLF component is likely to reflect changes in vasomotor tone in relation to thermoregulation and local adjustment of resistance in individual vascular beds; the LF component is considered to be a marker of sympathetic activity, although it remains a matter of debate; and the HF component mainly originates from respiratory activity and is considered to be mediated by vagal input (27). In rats, Cerutti et al. (8) determined that the LF component ranged between 0.27 and 0.74 Hz, and the HF component was > 0.75 Hz.

Averaged dynamic gain values of sympathetic transfer function for VLF and LF bands did not differ between the sedentary and exercised-trained groups (Fig. 4*A*). These results suggest that changes in the peripheral sympathetic control of HR likely do not contribute significantly to training-induced alterations in HRV. Therefore, the lower percentage of LF power and LF/HF ratio in the exercised-trained group (Table 2) may indicate reduced activation of sympathetic outflow from autonomic centers (23). In contrast, averaged dynamic gain values of vagal transfer function for VLF, LF, and HF bands (Fig. 4*B*) as

Table 4. *Sympathetic transfer function parameters and step response*

	Sedentary	Exercise Trained
Gain, beats·min^{-1}·Hz^{-1}	4.2 ± 1.5	4.5 ± 1.5
Natural frequency, Hz	0.07 ± 0.01	0.08 ± 0.01
Damping ratio	1.96 ± 0.55	1.69 ± 0.15
Lag time, s	0.71 ± 0.10	0.62 ± 0.11
Steady-state response, beats/min	3.6 ± 1.6	4.2 ± 1.2
80% rise time, s	12.9 ± 2.7	12.1 ± 3.0

Values are means ± SD. See APPENDIX for transfer function parameters.

Table 5. *AP and HR during dynamic vagal stimulation protocol*

	Sedentary		Exercise Trained	
	Prestimulation	During stimulation	Prestimulation	During stimulation
AP, mmHg	72 ± 21	68 ± 15	92 ± 14	80 ± 21
HR, beats/min	373 ± 18	327 ± 38 †	372 ± 14	301 ± 32 †

Values are means ± SD. †$P < 0.05$ compared with prestimulation.

Downloaded from ajpregu.physiology.org on January 23, 2012

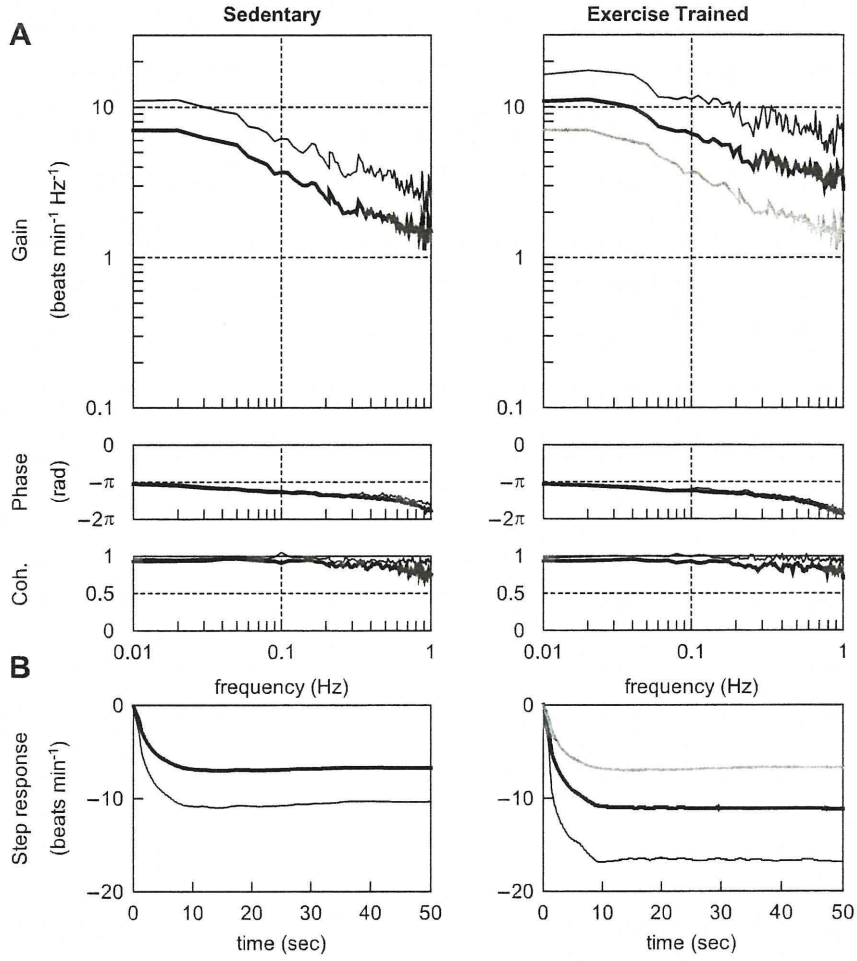

Fig. 3. *A*: transfer function from vagal stimulation to the HR response obtained in sedentary and exercised-trained rats. Gains (*top*), phase shifts (*middle*), and coherence functions (*bottom*) are presented. *B*: calculated step response to 1-Hz tonic vagal stimulation. Thick lines represent the mean, whereas thin lines indicate ± SD values. The gray solid curves in the gain and step response panels (*right*) duplicate the means (*left*).

well as the percentage of HF power (Table 2) were significantly greater in the exercised-trained compared with the sedentary group. These results suggest that the augmentation in HRV induced by exercise training is, at least in part, mediated by augmentations in the peripheral vagal control of HR.

What are the possible mechanisms underlying augmentations in the peripheral vagal control of HR? Danson and Paterson (10) have presented evidence that neuronal nitric oxide synthase may be a key enzymatic protein underlying such training-induced increases in cardiac vagal function. This group has also demonstrated that HR changes in response to vagal stimulation are enhanced by exercise training in wild-type mice but not in heterozygous neuronal nitric oxide synthase knockout mice (9). Another candidate for augmentations in the peripheral vagal control of HR is muscarinic receptors, which play a fundamental role in HR control via vagally mediated regulation. However, the effects of exercise training have been inconsistent among studies, showing both increases (12) and no change (2, 3) in muscarinic receptors in the myocardium of rats. The possibility cannot be dismissed that training-induced changes in the activity of afferent inputs mediating vagal outflow may also contribute to the alterations in HRV (4). Further investigation is needed to clarify these issues.

Table 6. *Vagal transfer function parameters and step response*

	Sedentary	Exercise Trained
Gain, beats·min^{-1}·Hz^{-1}	6.1 ± 3.0	9.7 ± 5.1#
Corner frequency, Hz	0.11 ± 0.05	0.17 ± 0.09
Lag time, s	0.10 ± 0.08	0.17 ± 0.08
Steady-state response, beats/min	−6.7 ± 3.6	−11.2 ± 5.7#
80% Fall time, s	4.3 ± 2.2	4.3 ± 1.5

Values are means ± SD. #P = 0.06 compared with sedentary group. See APPENDIX for transfer function parameters.

Perspectives and Significance

To date, the mechanisms underlying increased HRV after exercise training remain to be elucidated. HRV may reflect both the autonomic outflow from the central nervous system and the peripheral autonomic regulation of atrial pacemaker cells. In human studies, it is difficult to separately examine each factor. The findings of the present study suggest that the augmentation in HRV induced by exercise training is, at least in part, mediated by augmentations in the peripheral vagal control of HR. In other words, even if vagal outflow from the central nervous system remains unchanged after exercise training, HRV could be increased by an enhanced responsiveness in the peripheral vagal, but not sympathetic, regulation of HR.

Downloaded from ajpregu.physiology.org on January 23, 2012

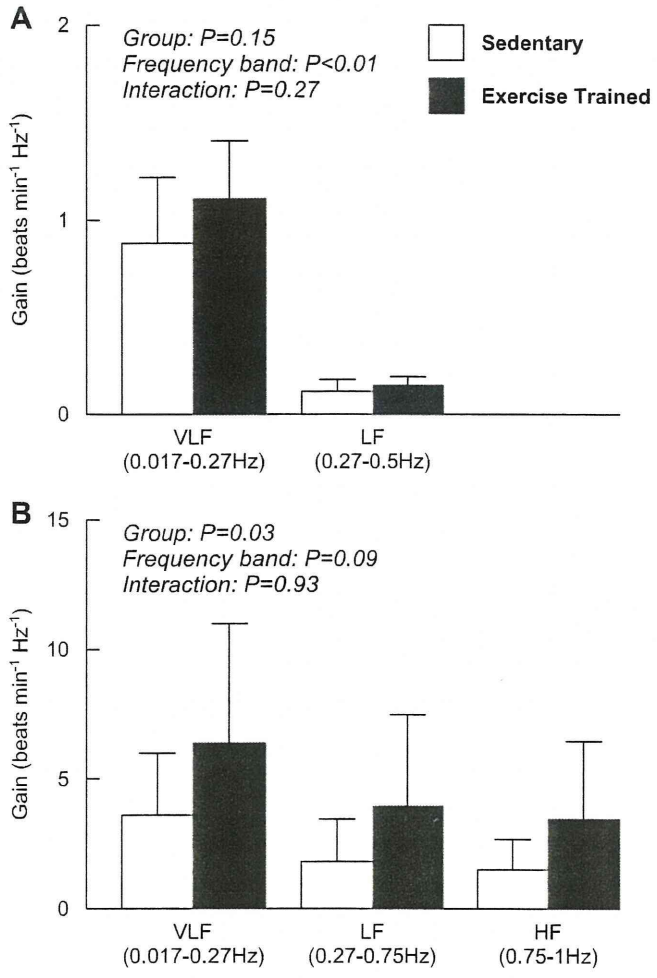

Fig. 4. Averaged sympathetic (*A*) and vagal (*B*) gain calculated from corresponding transfer function in very low frequency (VLF), low frequency (LF), and high frequency (HF) bands.

It has been well documented that decreased HRV is observed in heart failure (18) as well as in a variety of lifestyle-related diseases such as diabetes (16), hypertension (24), and obesity (1). Furthermore, reductions in HRV are related to increases in mortality rates as well as the occurrence of adverse cardiac events (32). Exercise training-induced augmentations in HRV maintain the potential to partially correct or normalize the autonomic dysfunction manifest in these disease states (4). Understanding the mechanisms contributing to the alterations in HRV induced by exercise training may significantly impact the development of novel therapeutic strategies for the treatment of autonomic dysfunction.

Limitations

There are several limitations to this study. First, the rats were slightly hyperventilated throughout the stimulation protocol. We cannot rule out the possibility that the hyperventilation might have affected the results reported. Second, dynamic sympathetic stimulation lowered mean AP in sedentary rats although sinoaortic barodenervation was performed. This may be explained by a possible difference in left ventricular functional capacity. For example, under conditions of equivalent HR, changes in systolic blood pressure were smaller in sedentary rats compared with exercised-trained rats (13). Third, the stimulation amplitude was fixed at 10 V for both sympathetic and vagal nerve stimulation. It should be noted, however, that our preliminary results indicated that 10 V was sufficiently large enough to evoke maximal HR responses. Fourth, transfer function data were obtained from anesthetized animals. This must be taken into account when interpreting the present results as anesthesia may affect the peripheral autonomic regulation of atrial pacemaker cells. Finally, we stimulated the sympathetic and vagal nerves according to a binary white noise signal. Although this method of stimulation is quite different from the physiological pattern of neuronal discharge, the coherence was near unity over the frequency range of interest. This finding indicates that the system properties do not vary considerably in response to different patterns of stimulation.

Conclusion

In the present study, it was demonstrated for the first time that exercise training did not alter dynamic sympathetic control of HR, while it did augment dynamic vagal control of HR. In addition, the group effect was significant with regard to the dynamic gain values for the vagal transfer functions corresponding to VLF, LF, and HF bands. This finding suggests that enhancements in the peripheral vagal control of HR may, at

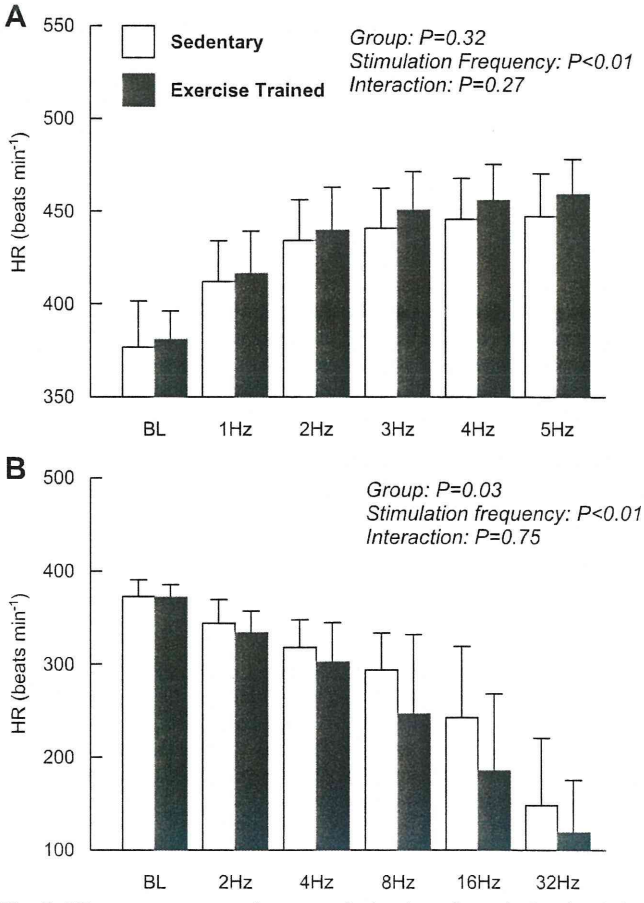

Fig. 5. HR response to stepwise sympathetic (*A*) and vagal (*B*) stimulation obtained in sedentary and exercised-trained rats.

Downloaded from ajpregu.physiology.org on January 23, 2012

least in part, contribute to the exercise-induced augmentation in HRV in healthy rats.

APPENDIX: TRANSFER FUNCTION ANALYSIS

The dynamic transfer function from binary white noise stimulation to the HR response was estimated based on the following procedure. Input-output data pairs of the stimulation frequency and HR were resampled at 10 Hz to be consistent with our previous study (21). Subsequently, data pairs were partitioned into eight 50% overlapping segments consisting of 1,024 data points each. For each segment, the linear trend was subtracted and a Hanning window was applied. A fast Fourier transform was then performed to obtain the frequency spectra of nerve stimulation [$N(f)$] and HR [$HR(f)$]. Over the eight segments, the power of the nerve stimulation [$S_{N\cdot N}(f)$], the power of the HR [$S_{HR\cdot HR}(f)$], and the cross-power between these two signals [$S_{N\cdot HR}(f)$] were ensemble averaged. Finally, the transfer function [$H(f)$] from nerve stimulation to the HR response was determined using the following equation (20).

$$H(f) = \frac{S_{N\text{-}HR}(f)}{S_{N\cdot N}(f)}$$

To quantify the linear dependence of the HR response on vagal or sympathetic stimulation, the magnitude-squared coherence function [Coh(f)] was estimated employing the following equation (20).

$$\mathrm{Coh}(f) = \frac{\left|S_{\mathrm{N\text{-}HR}}(f)\right|^2}{S_{\mathrm{N\cdot N}}(f)\cdot S_{\mathrm{HR\cdot HR}}(f)}$$

Coherence values range from zero to unity. Unity coherence indicates perfect linear dependence between the input and output signals; in contrast, zero coherence indicates total independence between the two signals.

Since the transfer function from sympathetic stimulation to HR response in rats approximated a second order low-pass filter with pure delay (21), we determined the parameters of the sympathetic transfer function using the following equation.

$$H(f) = \frac{K}{1 + 2\zeta\frac{f}{f_N}\mathrm{j} + \left(\frac{f}{f_N}\mathrm{j}\right)^2} e^{-2\pi f \mathrm{j} L}$$

where K is dynamic gain (in beats·min^{-1}·Hz^{-1}), f_N is the natural frequency (in Hz), ζ is the damping ratio, L is lag time (in s), and f and j represent frequency and imaginary units, respectively. These parameters were estimated by means of an iterative nonlinear least squares regression.

Since the transfer function from vagal stimulation to HR response in rats approximated a first-order, low-pass filter with pure delay (21), we determined the parameters of the vagal transfer function using the following equation.

$$H(f) = \frac{-K}{1 + \frac{f}{f_C}\mathrm{j}} e^{-2\pi f \mathrm{j} L}$$

where K represents the dynamic gain (in beats·min^{-1}·Hz^{-1}), f_C denotes the corner frequency (in Hz), L denotes the lag time (in s), and f and j represent frequency and imaginary units, respectively. The negative sign in the numerator indicates the negative HR response to vagal stimulation. These parameters were estimated by means of an iterative nonlinear least squares regression.

GRANTS

This study was supported by Health and Labor Sciences Research Grants H18-nano-Ippan-003, H19-nano-Ippan-009, H20-katsudo-Shitei-007, and H21-nano-Ippan-005 from the Ministry of Health, Labor and Welfare of Japan, by Grants-in-Aid for Scientific Research No. 19700559 from the Ministry of Education, Culture, Sports, Science and Technology in Japan, and by the Industrial Technology Research Grant Program from New Energy and Industrial Technology Development Organization of Japan. M. Mizuno was supported from Research Fellowships of the Japan Society for the Promotion of Science for Young Scientists.

DISCLOSURES

No conflicts of interest, financial or otherwise, are declared by the author(s).

REFERENCES

1. **Arone LJ, Mackintosh R, Rosenbaum M, Leibel RL, Hirsch J.** Autonomic nervous system activity in weight gain and weight loss. *Am J Physiol Regul Integr Comp Physiol* 269: R222–R225, 1995.
2. **Barbier J, Rannou-Bekono F, Marchais J, Berthon PM, Delamarche P, Carre F.** Effect of training on β1-, β2-, β3-adrenergic and M2 muscarinic receptors in rat heart. *Med Sci Sports Exerc* 36: 949–954, 2004.
3. **Barbier J, Reland S, Ville N, Rannou-Bekono F, Wong S, Carre F.** The effects of exercise training on myocardial adrenergic and muscarinic receptors. *Clin Auton Res* 16: 61–65, 2006.
4. **Billman GE.** Cardiac autonomic neural remodeling and susceptibility to sudden cardiac death: effect of endurance exercise training. *Am J Physiol Heart Circ Physiol* 297: H1171–H1193, 2009.
5. **Blomqvist CG, Saltin B.** Cardiovascular adaptations to physical training. *Annu Rev Physiol* 45: 169–189, 1983.
6. **Brenner DA, Apstein CS, Saupe KW.** Exercise training attenuates age-associated diastolic dysfunction in rats. *Circulation* 104: 221–226, 2001.
7. **Buch AN, Coote JH, Townend JN.** Mortality, cardiac vagal control and physical training–what's the link? *Exp Physiol* 87: 423–435, 2002.
8. **Cerutti C, Gustin MP, Paultre CZ, Lo M, Julien C, Vincent M, Sassard J.** Autonomic nervous system and cardiovascular variability in rats: a spectral analysis approach. *Am J Physiol Heart Circ Physiol* 261: H1292–H1299, 1991.
9. **Danson EJ, Mankia KS, Golding S, Dawson T, Everatt L, Cai S, Channon KM, Paterson DJ.** Impaired regulation of neuronal nitric oxide synthase and heart rate during exercise in mice lacking one nNOS allele. *J Physiol* 558: 963–974, 2004.
10. **Danson EJ, Paterson DJ.** Enhanced neuronal nitric oxide synthase expression is central to cardiac vagal phenotype in exercise-trained mice. *J Physiol* 546: 225–232, 2003.
11. **DiCarlo SE, Bishop VS.** Exercise training attenuates baroreflex regulation of nerve activity in rabbits. *Am J Physiol Heart Circ Physiol* 255: H974–H979, 1988.
12. **Favret F, Henderson KK, Clancy RL, Richalet JP, Gonzalez NC.** Exercise training alters the effect of chronic hypoxia on myocardial adrenergic and muscarinic receptor number. *J Appl Physiol* 91: 1283–1288, 2001.
13. **Fitzsimons DP, Bodell PW, Herrick RE, Baldwin KM.** Left ventricular functional capacity in the endurance-trained rodent. *J Appl Physiol* 69: 305–312, 1990.
14. **Goldsmith RL, Bigger JT Jr, Steinman RC, Fleiss JL.** Comparison of 24-hour parasympathetic activity in endurance-trained and untrained young men. *J Am Coll Cardiol* 20: 552–558, 1992.
15. **Hammond HK, White FC, Brunton LL, Longhurst JC.** Association of decreased myocardial β-receptors and chronotropic response to isoproterenol and exercise in pigs following chronic dynamic exercise. *Circ Res* 60: 720–726, 1987.
16. **Ikeda T, Matsubara T, Sato Y, Sakamoto N.** Circadian blood pressure variation in diabetic patients with autonomic neuropathy. *J Hypertens* 11: 581–587, 1993.
17. **Kawada T, Ikeda Y, Sugimachi M, Shishido T, Kawaguchi O, Yamazaki T, Alexander J Jr, Sunagawa K.** Bidirectional augmentation of heart rate regulation by autonomic nervous system in rabbits. *Am J Physiol Heart Circ Physiol* 271: H288–H295, 1996.
18. **La Rovere MT, Pinna GD, Maestri R, Mortara A, Capomolla S, Febo O, Ferrari R, Franchini M, Gnemmi M, Opasich C, Riccardi PG, Traversi E, Cobelli F.** Short-term heart rate variability strongly predicts sudden cardiac death in chronic heart failure patients. *Circulation* 107: 565–570, 2003.

Downloaded from ajpregu.physiology.org on January 23, 2012

19. **Malliani A, Pagani M, Lombardi F, Cerutti S.** Cardiovascular neural regulation explored in the frequency domain. *Circulation* 84: 482–492, 1991.
20. **Marmarelis P, Marmarelis V.** The white noise method in system identification. In: *Analysis of Physiological Systems*. New York: Plenum, 1978, p. 131–221.
21. **Mizuno M, Kawada T, Kamiya A, Miyamoto T, Shimizu S, Shishido T, Smith SA, Sugimachi M.** Dynamic characteristics of heart rate control by the autonomic nervous system in rats. *Exp Physiol* 95: 919–925, 2010.
22. **Mohan RM, Choate JK, Golding S, Herring N, Casadei B, Paterson DJ.** Peripheral pre-synaptic pathway reduces the heart rate response to sympathetic activation following exercise training: role of NO. *Cardiovasc Res* 47: 90–98, 2000.
23. **Mueller PJ.** Exercise training attenuates increases in lumbar sympathetic nerve activity produced by stimulation of the rostral ventrolateral medulla. *J Appl Physiol* 102: 803–813, 2007.
24. **Mussalo H, Vanninen E, Ikaheimo R, Laitinen T, Laakso M, Lansimies E, Hartikainen J.** Heart rate variability and its determinants in patients with severe or mild essential hypertension. *Clin Physiol* 21: 594–604, 2001.
25. **Negrao CE, Moreira ED, Santos MC, Farah VM, Krieger EM.** Vagal function impairment after exercise training. *J Appl Physiol* 72: 1749–1753, 1992.
26. **Nieto JL, Laviada ID, Guillen A, Haro A.** Adenylyl cyclase system is affected differently by endurance physical training in heart and adipose tissue. *Biochem Pharmacol* 51: 1321–1329, 1996.
27. **Pagani M, Lombardi F, Guzzetti S, Rimoldi O, Furlan R, Pizzinelli P, Sandrone G, Malfatto G, Dell'Orto S, Piccaluga E.** Power spectral analysis of heart rate and arterial pressure variabilities as a marker of sympatho-vagal interaction in man and conscious dog. *Circ Res* 59: 178–193, 1986.
28. **Sandercock GR, Bromley PD, Brodie DA.** Effects of exercise on heart rate variability: inferences from meta-analysis. *Med Sci Sports Exerc* 37: 433–439, 2005.
29. **Schwarz P, Diem R, Dun NJ, Forstermann U.** Endogenous and exogenous nitric oxide inhibits norepinephrine release from rat heart sympathetic nerves. *Circ Res* 77: 841–848, 1995.
30. **Souza SB, Flues K, Paulini J, Mostarda C, Rodrigues B, Souza LE, Irigoyen MC, De Angelis K.** Role of exercise training in cardiovascular autonomic dysfunction and mortality in diabetic ovariectomized rats. *Hypertension* 50: 786–791, 2007.
31. **Tezini GC, Silveira LC, Villa-Cle PG Jr, Jacinto CP, Di Sacco TH, Souza HC.** The effect of aerobic physical training on cardiac autonomic control of rats submitted to ovariectomy. *Menopause* 16: 110–116, 2009.
32. **Tsuji H, Larson MG, Venditti FJ Jr, Manders ES, Evans JC, Feldman CL, Levy D.** Impact of reduced heart rate variability on risk for cardiac events. The Framingham Heart Study. *Circulation* 94: 2850–2855, 1996.
33. **Werle EO, Strobel G, Weicker H.** Decrease in rat cardiac β1- and β2-adrenoceptors by training and endurance exercise. *Life Sci* 46: 9–17, 1990.
34. **Williams RS.** Physical conditioning and membrane receptors for cardioregulatory hormones. *Cardiovasc Res* 14: 177–182, 1980.
35. **Williams RS, Schaible TF, Bishop T, Morey M.** Effects of endurance training on cholinergic and adrenergic receptors of rat heart. *J Mol Cell Cardiol* 16: 395–403, 1984.
36. **Yamamoto K, Miyachi M, Saitoh T, Yoshioka A, Onodera S.** Effects of endurance training on resting and post-exercise cardiac autonomic control. *Med Sci Sports Exerc* 33: 1496–1502, 2001.

Downloaded from ajpregu.physiology.org on January 23, 2012

Autonomic Neuroscience: Basic and Clinical xxx (2010) xxx–xxx

Contents lists available at ScienceDirect

Autonomic Neuroscience: Basic and Clinical

journal homepage: www.elsevier.com/locate/autneu

Involvement of the mechanoreceptors in the sensory mechanisms of manual and electrical acupuncture

Hiromi Yamamoto [a,*], Toru Kawada [b], Atsunori Kamiya [b], Shunichi Miyazaki [a], Masaru Sugimachi [b]

[a] Division of Cardiology, Department of Medicine, Faculty of Medicine, Kinki University, Osaka, Japan
[b] Department of Cardiovascular Dynamics, National Cerebral and Cardiovascular Center Research Institute, Osaka, Japan

ARTICLE INFO

Article history:
Received 21 April 2010
Received in revised form 27 September 2010
Accepted 4 November 2010
Available online xxxx

Keywords:
Acupuncture
Arterial blood pressure
Heart rate
Mechanoreceptor
Gadolinium
Aortic depressor nerve

ABSTRACT

The modalities of acupuncture can be broadly classified into manual acupuncture (MA) and electroacupuncture (EA). Although MA has been reported to cause winding of tissue around the needle and subsequent activation of the sensory mechanoreceptors and nociceptors, the sensory mechanisms of acupuncture stimulation are not fully understood. To test the hypothesis that the involvement of the mechanoreceptors in the sensory mechanism is different in MA and EA, we examined the effects of a stretch-activated channel blocker gadolinium on the hemodynamic responses to hind limb MA and EA in anesthetized rats (n=9). Gadolinium significantly attenuated the MA-induced bradycardic response (−22±5 vs. −10±3 bpm, P<0.05) and tended to attenuate the MA-induced depressor response (−30±5 vs. −18±4 mm Hg, P=0.06). On the other hand, gadolinium significantly attenuated both the EA-induced bradycardic (−22±5 vs. −9±4 bpm, P<0.01) and depressor responses (−32±6 vs. −15±5 mm Hg, P<0.01). These results indicate that the mechanoreceptors are involved in the sensory mechanisms for both MA and EA.

© 2010 Published by Elsevier B.V.

1. Introduction

Acupuncture has been used to modulate autonomic nervous activity and cardiovascular function (Kimura and Sato, 1997; Lin et al., 2001). The modalities of acupuncture can be broadly classified into two categories: manual acupuncture (MA) and electroacupuncture (EA). MA and EA induce similar changes in the functional magnetic resonance imaging signal in the human brain (Napadow et al., 2005). Neural mechanisms involved in acupuncture have been the focus of investigations. The effects of EA are considered to be related to stimulation of finely myelinated (group III) and unmyelinated (group IV) fibers, which activate opioid receptors in the rostral ventrolateral medulla to inhibit sympathetic outflow (Chao et al., 1999). Depletion of group IV fibers by neonatal capsaicin treatment reduces the influence of EA on the pressor responses to mechanical stimulation of visceral organs (Tjen-A-Looi et al., 2005). The extensive network of tangential cutaneous axons, coupled with their communications with the large numbers of Merkel cells, might be considered a new division of the autonomic nervous system: the cutaneous intrinsic visceral afferent nervous system (Silberstein, 2009).

Although cardiovascular responses induced by acupuncture-like stimulation are known to be reflexes mediated via somatic afferent nerves, visceral afferent nerves and autonomic efferent nerves (Sato et al., 1994, 2002; Tjen-A-Looi et al., 2005; Uchida et al., 2007; Yamamoto et al., 2008; Silberstein, 2009), the sensory mechanisms of MA and EA that initiate afferent nerve discharge are not fully understood. Langevin et al. (2001) proposed that MA causes winding of tissues around the needle and subsequent activation of sensory mechanoreceptors and nociceptors, and also suggested that changes in extracellular milieu induced by MA are important factors for neuromodulation. Burnstock (2009) proposed that mechanical deformation of the skin leads to the release of ATP from keratinocytes, fibroblasts and other cells; then the sensory nerves are activated through purinergic receptors. Although EA may induce MA-like stimuli via electrical twitching of surrounding tissues, EA may also directly depolarize sensory axons and nerve terminals adjacent to the needle and induce reflex responses. If the direct depolarization is the major sensory mechanism of EA, inhibition of mechanoreceptors would not zsignificantly attenuate the effects of EA. On the other hand, if the mechanical stimulation plays a dominant role in the sensory mechanism of EA, inhibition of mechanoreceptors would significantly attenuate the effects of EA.

Among mechanoreceptors, mechanosensitive ion channels detect mechanical stimuli and transduce these stimuli into electrical signals in sensory neurons. Gadolinium chloride is widely used experimentally as an inhibitor of stretch-activated ion channels and physiological responses of tissues to mechanical stimulation (Adding et al., 2001). To test the hypothesis that the contribution of mechanoreceptors in the sensory mechanism differs in MA and EA, we examined the effects of gadolinium on the hemodynamic responses to MA and EA in anesthetized rats.

* Corresponding author. 377-2 Ohno-higashi, Osaka-sayama, Osaka 589-8511, Japan. Tel.: +81 72 366 0221; fax: +81 72 368 2378.
E-mail address: hiromi@med.kindai.ac.jp (H. Yamamoto).

1566-0702/$ – see front matter © 2010 Published by Elsevier B.V.
doi:10.1016/j.autneu.2010.11.004

Please cite this article as: Yamamoto, H., et al., Involvement of the mechanoreceptors in the sensory mechanisms of manual and electrical acupuncture, Auton. Neurosci. (2010), doi:10.1016/j.autneu.2010.11.004

ARTICLE IN PRESS

2. Methods

2.1. Surgical preparation

Animal care was provided in strict accordance with the Guiding Principles for the Care and Use of Animals in the Field of Physiological Sciences approved by the Physiological Society of Japan. All protocols were reviewed and approved by the Animal Subject Committee at the National Cerebral and Cardiovascular Center. Male Wister Kyoto rats weighing from 310 to 460 g were anesthetized by an intraperitoneal injection of pentobarbital sodium (50 mg/kg) and ventilated mechanically via a tracheal tube with oxygen-enriched room air. The depth of anesthesia was maintained by continuous intravenous infusion of pentobarbital sodium (20–25 mg kg^{-1} h^{-1}) through a double lumen catheter inserted into the right external carotid vein. Ringer solution (6 mg kg^{-1} h^{-1}) was administered to maintain fluid balance. Arterial blood pressure (AP) was measured using a catheter inserted into the right common carotid artery. Heart rate (HR) was determined from AP using a cardiotachometer. Body temperature was maintained at approximately 38 °C using a heating pad.

2.2. MA and EA stimulations ($n=9$)

With the animal in the supine position, both hind limbs were lifted to obtain a better view of the lateral sides of the lower legs. An acupuncture needle with a diameter of 0.2 mm (CE0123, Seirin-Kasei, Japan) was inserted into a point below the knee joint just lateral to the tibia in the left or right leg. For MA stimulation, the acupuncture needle was inserted to a depth of 5–10 mm and manually twisted clockwise and counter-clockwise, and moved up and down at a frequency of 1–2 Hz for a duration of 120 s. Two to three MA trials were conducted with an intervening interval of more than 5 min within which AP and HR returned to the respective pre-stimulation values. For EA stimulation, another acupuncture needle was inserted into a point approximately 1 cm from the above-mentioned needle toward the ankle joint and used as the ground. EA was applied for 120 s using an isolator connected to an electrical stimulator (SEN 7203, Nihon Kohden, Japan). The pulse width and the stimulus current were set at 500 μs and 5 mA, respectively. The stimulation frequency was set at 10 Hz in six and at 20 Hz in three of the nine rats. The pulse duration was based on previous studies (Tjen-A-Looi et al., 2005; Yamamoto et al., 2008; Uchida et al., 2008). The amplitude and frequency were selected so that the magnitudes of reflex hemodynamic responses became comparable to those induced by MA before gadolinium administration. In each animal, two to three EA trials were conducted with an intervening interval of more than 5 min within which AP and HR returned to the respective pre-stimulation values.

Gadolinium chloride hexahydrate was dissolved in saline at a concentration of 20 mM (Nakamoto and Matsukawa, 2007). After performing MA and EA under control conditions, we administered the gadolinium solution intravenously (2 ml/kg). After 10 min, we repeated MA and EA. The acupuncture needle positions were kept unchanged between MA and EA trials as well as before and after the gadolinium administration.

In a supplemental protocol ($n=7$ additional rats), to examine the possibility that simple insertion of needles caused significant hemodynamic influences, an acupuncture needle (CE0123, Seirin-Kasei, Japan) was only inserted into a point below the knee joint just lateral to the tibia in the left or right leg and placed for a duration of 120 s. Needle was inserted to a depth of 5–10 mm.

2.3. Aortic depressor nerve stimulation ($n=6$)

Using a pair of platinum electrodes, we identified the aortic depressor nerve (ADN) running along the common carotid artery, based on the AP pulse-synchronous nerve activity monitored through a loud speaker. After a depressor response to brief electrical stimulation of the nerve was confirmed, the electrodes and the nerve were fixed and insulated by silicone glue (Kwik-Sil, World Precision Instruments, FL, USA). The nerve fibers caudal to the electrodes were then crushed by a tight ligature so that only the afferent fibers directed to the central nervous system were stimulated. In four of the six rats, the right ADN was stimulated. In the remaining two rats, the left ADN was stimulated because of failure to stimulate the right ADN properly. The ADN was stimulated for 120 s at a frequency of 50 Hz (pulse width: 2 ms, voltage: 2 V). ADN stimulation was repeated with an interval of 5 min until the AP and HR responses appeared to be reproducible under control conditions. We then administered the gadolinium solution intravenously (20 mM, 2 ml/kg). After 10 min, we repeated the ADN stimulation.

2.4. Data analysis

Data were digitized using a 16-bit analog-to-digital converter (Contec, Japan) and stored at 200 Hz on a laboratory computer system. First, AP and HR data were averaged every 10 s. Averaged time courses of AP and HR responses were then obtained from two to three trials of MA, EA or ADN stimulation in each animal. Next, the effects of MA, EA or ADN were examined using repeated-measures one-way analysis of variance (ANOVA) followed by Dunnett's test (Glantz, 2002). The baseline data point immediately before stimulation was treated as a single control point for the Dunnett's test. Finally, the maximum effect of MA, EA or ADN stimulation was quantified by the differences between the minimum and baseline values for AP and HR (ΔAP and ΔHR). The effects of gadolinium on ΔAP and ΔHR were examined by a paired-t test (Glantz, 2002). The differences were considered significant at $P<0.05$. Data are presented in mean ± SE values.

3. Results

Fig. 1 depicts the averaged time courses of AP and HR responses to MA ($n=9$ rats). MA gradually decreased AP and HR under control conditions. The minimum AP and HR were reached near the end of the MA stimulation period. After the cessation of MA, AP and HR gradually returned toward the respective baseline values. Intravenous gadolinium administration significantly decreased baseline AP from 138 ± 5 to 120 ± 5 mm Hg ($P<0.01$) but had no significant effect on baseline HR (379 ± 10 vs. 383 ± 7 bpm). Following gadolinium administration, although MA also decreased AP and HR significantly, ΔAP tended to be attenuated (−30 ± 5 vs. −18 ± 4 mm Hg; 68 ± 16% of the pre-gadolinium; $P=0.06$) and ΔHR was significantly attenuated (−22 ± 5 vs. −10 ± 3 bpm; 57 ± 23% of the pre-gadolinium; $P<0.05$) compared to control conditions.

Fig. 2 depicts the averaged time courses of AP and HR responses to EA ($n=9$ rats). Under control conditions, EA decreased AP and HR. Both responses reached almost a steady state at approximately 1 min of EA stimulation. AP and HR remained decreased during the rest of the EA stimulation period, and gradually returned toward the respective baseline values after the cessation of EA. Intravenous gadolinium administration significantly decreased baseline AP from 140 ± 5 to 123 ± 7 mm Hg ($P<0.01$) but did not affect baseline HR (385 ± 9 vs. 384 ± 7 bpm). Following gadolinium administration, although EA significantly decreased AP, the decrease in HR was only significant at 55 s of EA stimulation. ΔAP (−32 ± 6 vs. −15 ± 5 mm Hg; 38 ± 11% of the pre-gadolinium; $P<0.01$) and ΔHR (−22 ± 5 vs. −9 ± 4 bpm; 37 ± 14% of the pre-gadolinium; $P<0.01$) were attenuated significantly compared to control conditions.

In the supplemental protocol ($n=7$ rats), the insertion of an acupuncture needle alone did not significantly change AP (138 ± 9 vs. 138 ± 9 mm Hg) or HR (399 ± 20 vs. 400 ± 20 bpm).

Fig. 3 shows the averaged time courses of AP and HR responses to ADN stimulation ($n=6$ rats). ADN stimulation decreased AP and HR under control conditions. The minimum AP and HR were reached at 15 s of ADN stimulation. Both parameters remained decreased during the rest of the ADN stimulation period, and returned toward the respective

Please cite this article as: Yamamoto, H., et al., Involvement of the mechanoreceptors in the sensory mechanisms of manual and electrical acupuncture, Auton. Neurosci. (2010), doi:10.1016/j.autneu.2010.11.004

ARTICLE IN PRESS

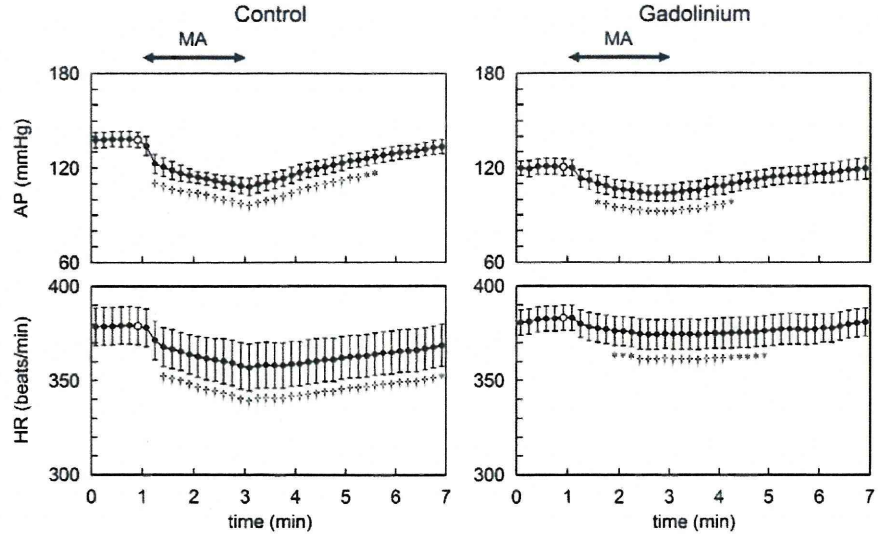

Fig. 1. Time courses of arterial pressure (AP) and heart rate (HR) responses induced by manual acupuncture (MA) averaged from 9 rats. MA gradually decreased AP and HR under control conditions (left) and after gadolinium administration (right). Gadolinium treatment tended to attenuate the AP response and significantly attenuated the HR response induced by MA, compared to control conditions. Data are mean ± SE values. $^{*}P<0.05$ and $^{\dagger}P<0.01$ versus the control data point (open circle) immediately before the application of MA.

baseline values after the cessation of ADN stimulation. AP and HR appeared to recover more rapidly compared to those observed after MA and EA. Intravenous gadolinium administration significantly decreased baseline AP from 126 ± 4 to 118 ± 2 mm Hg ($P<0.01$) but had no significant effect on baseline HR (373 ± 13 vs. 369 ± 11 bpm). Following gadolinium administration, ADN stimulation significantly decreased AP and HR. Neither ΔAP (−43 ± 7 vs. −49 ± 3 mm Hg) nor ΔHR (−27 ± 8 vs. −34 ± 5 bpm) was attenuated compared to control conditions.

4. Discussion

We have shown that ion channels blocked by gadolinium are implicated in the hypotensive and bradycardic effects of acupuncture at the hind limb in rats, irrespective of technique.

4.1. Effects of gadolinium on AP and HR responses to MA and EA

Insertion of acupuncture needle alone did not change AP and HR significantly, indicating that continuous stimulation either by MA or EA was necessary to induce sustained AP and HR responses. Mechanoreceptors are thought to play an important role in the sensory mechanism of MA. Because gadolinium blocks mechanosensitive ion channels in sensory neurons (Cho et al., 2002), we hypothesized that intravenous administration of gadolinium would attenuate the AP and HR responses to MA. As expected, ΔAP tended to be attenuated after gadolinium administration (Fig. 1, top). However, since gadolinium also decreased baseline AP, it is uncertain whether the attenuation of ΔAP was mainly attributable to the inhibition of reflex response to MA or to the decreased baseline AP. On the other hand, gadolinium did not significantly affect baseline HR and

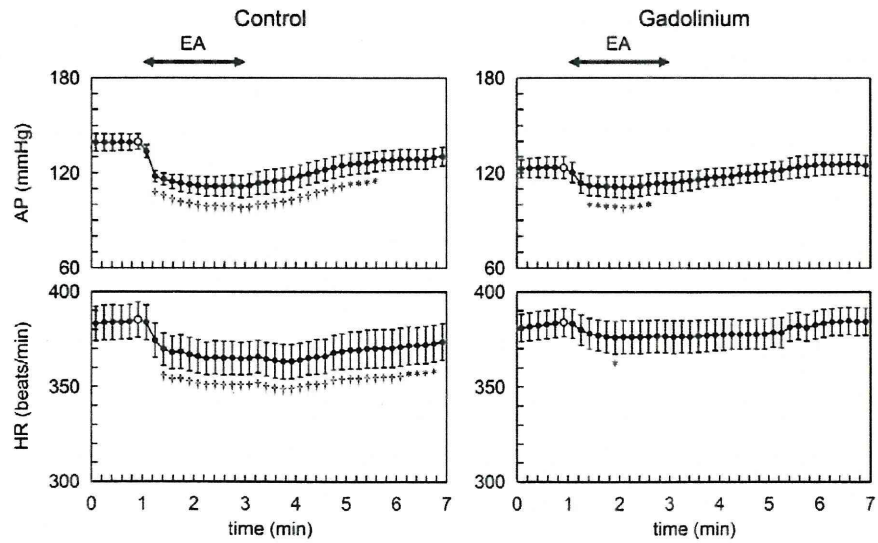

Fig. 2. Time courses of AP and HR responses induced by electroacupuncture (EA) averaged from 9 rats. EA gradually decreased AP and HR under control conditions (left) and after gadolinium administration (right). Gadolinium significantly attenuated both AP and HR responses induced by EA, compared to control conditions. Data are mean ± SE values. $^{*}P<0.05$ and $^{\dagger}P<0.01$ versus the control data point (open circle) immediately before the application of EA.

Please cite this article as: Yamamoto, H., et al., Involvement of the mechanoreceptors in the sensory mechanisms of manual and electrical acupuncture, Auton. Neurosci. (2010), doi:10.1016/j.autneu.2010.11.004

ARTICLE IN PRESS

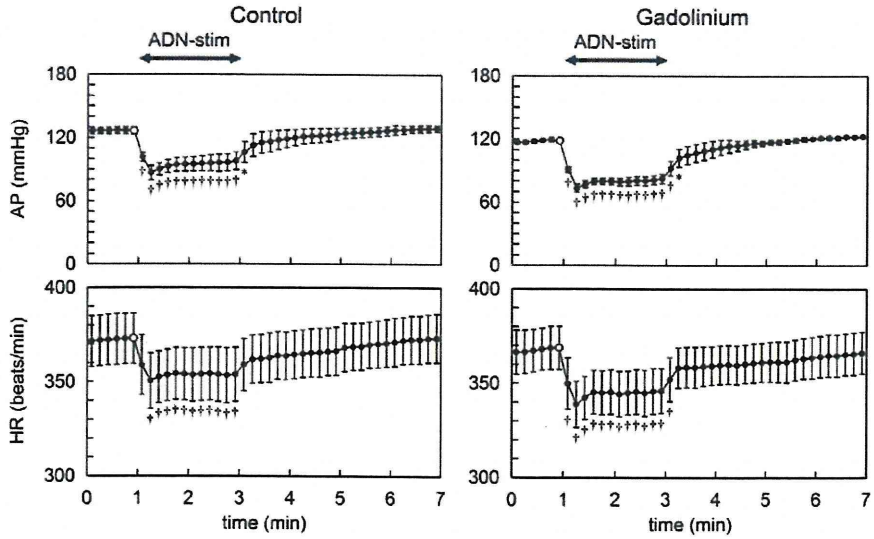

Fig. 3. Time courses of AP and HR responses induced by electrical stimulation of the aortic depressor nerve (ADN-stim) averaged from 6 rats. ADN-stim decreased AP and HR under control conditions (left) and after gadolinium administration (right). Gadolinium did not attenuate the AP and HR responses induced by ADN-stim, compared to control conditions. Data are mean ± SE values. $^{*}P<0.05$ and $^{\dagger}P<0.01$ versus the control data point (open circle) immediately before the application of ADN-stim.

significantly attenuated ΔHR induced by MA (Fig. 1, bottom). Judging from the HR response, it is conceivable that gadolinium inhibits the reflex hemodynamic responses to MA.

We assumed that direct depolarization of sensory axons and nerve terminals adjacent to the needle could be the major sensory mechanism of EA. In fact, direct electrical stimulation of muscle afferent fibers evokes a variety of cardiovascular responses similar to those induced by EA (Sato et al., 1981). If direct depolarization is the major sensory mechanism for EA, inhibition of mechanoreceptors would have no significant effect on EA, because the results of the ADN stimulation protocol indicates that the axonal conduction would not be blocked even after gadolinium administration once the afferent nerve is discharged (Fig. 3). Contrary to this assumption, gadolinium significantly attenuated ΔAP and ΔHR induced by EA (Fig. 2), suggesting that the mechanoreceptors play an important role in the sensory mechanism of EA, as in the case of MA. EA probably causes electrical twitching of surrounding tissues and exerts MA-like stimulation through the mechanoreceptors.

Despite the significant contribution of mechanoreceptors to the sensory mechanisms of both MA and EA, the fact that the hemodynamic responses to MA and EA were not entirely abrogated after gadolinium administration indicates the presence of sensory mechanisms other than the mechanosensitive ion channels. Not all capsaicin-sensitive neurons are mechanosensitive, and gadolinium has no effect on capsaicin-induced calcium transient in sensory neurons (Gschossmann et al., 2000). Depletion of group IV fibers by neonatal capsaicin treatment reduces the influence of EA on the pressor responses to mechanical stimulation of visceral organs (Tjen-A-Looi et al., 2005), suggesting an importance of capsaicin-sensitive neurons in the mechanisms of acupuncture. Nociceptive neurons are therefore a likely candidate for the residual sensory mechanism after gadolinium administration. The group IV C-fiber tactile afferents is known to be widely distributed in the skin of mammals (Wessberg et al., 2003). These fibers could be regarded as a cutaneous intrinsic visceral afferent nervous system (Silberstein, 2009). In addition, the present results do not rule out the possibility that direct depolarization of sensory axons or nerve terminals occurs during EA. Albeit this assumption, EA seemed to have received even greater influence from gadolinium than MA (Figs. 1 and 2). Because MA with needle movements can cause greater deformations in the adjacent extracellular milieu compared to EA, MA may have induced signal transductions other than mechanosensitive ion channels, such as integrin-linked signal transduction pathways (Aplin et al., 1998), resulting in the greater residual hemodynamic responses after gadolinium administration. Further studies are required in the future to solve this question.

4.2. Effects of gadolinium on the AP and HR responses to ADN stimulation

Gadolinium decreased baseline AP, suggesting actions other than the inhibition of mechanosensitive ion channels. For instance, gadolinium has been shown to block voltage-gated calcium, sodium and potassium channels (Adding et al., 2001). To exclude the possibility that gadolinium attenuates the reflex hemodynamic responses to MA and EA via nonspecific mechanisms such as the inhibition of central autonomic neurotransmission, we performed the ADN stimulation experiment. Gadolinium did not attenuate ΔAP and ΔHR induced by ADN stimulation (Fig. 3). It is unlikely, therefore, that gadolinium inhibits the central autonomic neurotransmission from afferent to efferent nerve activities or significantly blunted the AP and HR responses to changes in autonomic nerve activities.

4.3. Implication of MA and EA

Although the present results indicate that MA and EA may share a common sensory mechanism, EA may be more flexible than MA in terms of its application for biomedical engineering because the effects of EA can be controlled quantitatively by adjusting the stimulation current and stimulation frequency. As an example, a previous study from our laboratories has demonstrated that servo-controlled hind limb electrical stimulation can reduce AP at a prescribed target level in anesthetized cats (Kawada et al., 2009). EA can be applied continuously using a stimulating device without the attendance of an acupuncturist once the needle is properly positioned. Continuous electrical stimulation of auricular acupuncture points for 48 h/week has been shown to be more effective than auricular acupuncture without electrical stimulation for the treatment of chronic cervical pain in an outpatient population (Sator-Katzenschlager et al., 2003). Although further studies are required, EA delivered via a dedicated stimulating device may be an additional modality to the treatment of cardiovascular diseases.

4.4. Limitations

First, the present study was conducted under pentobarbital anesthesia. Because anesthesia affects the autonomic tone, AP and HR

Please cite this article as: Yamamoto, H., et al., Involvement of the mechanoreceptors in the sensory mechanisms of manual and electrical acupuncture, Auton. Neurosci. (2010), doi:10.1016/j.autneu.2010.11.004

ARTICLE IN PRESS

responses may differ when different anesthetics are used or when the animals are in a conscious state. However, as we compared the effects of gadolinium on the reflex responses to MA and EA under the same anesthetic conditions, the interpretation of the sensory mechanisms for MA and EA should be valid. Second, we performed EA at frequencies of 10 or 20 Hz in order to obtain AP and HR responses comparable to those observed during MA under control conditions. Because the effects of EA may differ depending on the magnitude of stimulation including pulse duration, current and frequency (Uchida et al., 2008; Kawada et al., 2009), further studies are needed to examine whether the effects of gadolinium on EA-induced hemodynamic responses vary depending on the stimulation intensities.

4.5. Conclusion

Intravenous administration of gadolinium attenuated the AP and HR responses to both MA and EA, suggesting that the mechanosensitive ion channels are involved in the sensory mechanisms of both MA and EA. EA may cause electrical twitching of surrounding tissues and induce MA-like stimulation through mechanoreceptors.

Acknowledgments

This study was supported by Health and Labour Sciences Research Grants (H19-nano-lppan-009, H20-katsudo-Shitei-007, and H21-nano-lppan-005) from the Ministry of Health, Labour and Welfare of Japan; by a Grant-in-Aid for Scientific Research (No. 20390462) from the Ministry of Education, Culture, Sports, Science and Technology of Japan; and by the Industrial Technology Research Grant Program from the New Energy and Industrial Technology Development Organization (NEDO) of Japan.

Appendix A

In an attempt to demonstrate that gadolinium does not significantly affect the hemodynamic responses to direct nerve stimulation related to acupuncture at the hind limb, we performed an additional protocol of tibial nerve stimulation in 5 anesthetized rats. The right tibial nerve was exposed and placed on a pair of platinum electrodes, and was stimulated for 120 s (500 μs, 10 Hz, 2 or 5 mA). ΔAP was -10.5 ± 3.5 mm Hg under baseline conditions, which was attenuated to -8.2 ± 4.4 mm Hg after gadolinium administration ($74 \pm 15\%$ of the pre-gadolinium, $P<0.01$). Although the relative reduction seemed smaller than that observed in EA ($38 \pm 11\%$ of the pre-gadolinium, see main text), because the reduction of ΔAP could be partly attributable to the decreased baseline AP after gadolinium administration, we could not judge whether gadolinium had truly inhibited the hypotensive effect of tibial nerve stimulation. Unfortunately, the tibial nerve stimulation did not change HR significantly in our experimental conditions ($\Delta HR = -1.1 \pm 4.4$ bpm before gadolinium vs. $\Delta HR = -1.4 \pm 4.1$ bpm after gadolinium), as opposed to a previous study (Uchida et al., 2008). As a result, we could not judge the effect of gadolinium based on HR either. We think the ADN stimulation protocol in the main text would be a second best surrogate to indicate the inability of gadolinium to block hemodynamic responses induced by direct activation of the afferent nerve.

References

Adding, L.C., Bannenberg, G.L., Gustafsson, L.E., 2001. Basic experimental studies and clinical aspects of gadolinium salts and chelates. Cardiovasc. Drug Rev. 19, 41–56.
Aplin, A.E., Howe, A., Alahari, S.K., Juliano, R.L., 1998. Signal transduction and signal modulation by cell adhesion receptors: the role of integrins, cadherins, immunoglobulin-cell adhesion molecules, and selectins. Pharmacol. Rev. 50 (2), 197–263.
Burnstock, G., 2009. Acupuncture: a novel hypothesis for the involvement of purinergic signalling. Med. Hypotheses 73, 470–472.
Cho, H., Shin, J., Shin, C.Y., Lee, S., Oh, U., 2002. Mechanosensitive ion channels in cultured sensory neurons of neonatal rats. J. Neurosci. 22 (4), 1238–1247.
Glantz, S.A., 2002. Primer of Biostatistics, 5th ed. McGraw-Hill, New York.
Gschossmann, J.M., Chaban, V.V., McRoberts, J.A., Raybould, H.E., Young, S.H., Ennes, H.S., Lembo, T., Mayer, E.A., 2000. Mechanical action of dorsal root ganglion cells in vitro: comparison with capsaicin and modulation by kappa-opioids. Brain Res. 856 (1–2), 101–110.
Kawada, T., Shimizu, S., Yamamoto, T., Shishido, T., Kamiya, A., Miyamoto, T., Sunagawa, K., Sugimachi, M., 2009. Servo-controlled hind-limb electrical stimulation for short-term arterial pressure control. Circ. J. 73 (5), 851–859.
Kimura, A., Sato, A., 1997. Somatic regulation of autonomic functions in anesthetized animals—neural mechanisms of physical therapy including acupuncture. Jpn J. Vet. Res. 45 (3), 137–145.
Langevin, H.M., Churchill, D.L., Cipolla, M.J., 2001. Mechanical signaling through connective tissue: a mechanism for the therapeutic effect of acupuncture. FASEB J. 15, 2275–2285.
Lin, M.C., Nahin, R., Gershwin, M.E., Longhurst, J.C., Wu, K.K., 2001. State of complementary and alternative medicine in cardiovascular, lung, and blood research: executive summary of a workshop. Circulation 103 (16), 2038–2041.
Nakamoto, T., Matsukawa, K., 2007. Muscle mechanosensitive receptors close to the myotendinous junction of the Achilles tendon elicit a pressor reflex. J. Appl. Physiol. 102, 2112–2120.
Napadow, V., Makris, N., Liu, J., Kettner, N.W., Kenneth, K.K., Hui, K.K.S., 2005. Effects of electroacupuncture versus manual acupuncture on the human brain as measured by fMRI. Hum. Brain Mapp. 24, 193–205.
Sato, A., Sato, Y., Schmidt, R.F., 1981. Heart rate changes reflecting modifications of efferent cardiac sympathetic outflow by cutaneous and muscle afferent volleys. J. Auton. Nerv. Syst. 4 (3), 231–247.
Sato, A., Sato, Y., Suzuki, A., Uchida, S., 1994. Reflex modulation of gastric and vesical function by acupuncture-like stimulation in anesthetized rats. Biomed. Res. 15, 59–65.
Sato, A., Sato, Y., Uchida, S., 2002. Reflex modulation of visceral functions by acupuncture-like stimulation in anesthetized rats. Int. Congr. Ser. 1238, 111–123.
Sator-Katzenschlager, S.M., Szeles, J.C., Scharbert, G., Michalek-Sauberer, A., Kober, A., Heinze, G., Kozek-Langenecker, S.A., 2003. Electrical stimulation of auricular acupuncture points is more effective than conventional manual auricular acupuncture in chronic cervical pain: a pilot study. Anesth. Analg. 97, 1469–1473.
Silberstein, M., 2009. The cutaneous intrinsic visceral afferent nervous system: a new model for acupuncture analgesia. J. Theor. Biol. 261, 637–642.
Tjen-A-Looi, S.C., Fu, L.-W., Zhou, W., Syuu, Z., Longhurst, J.C., 2005. Role of unmyelinated fibers in electroacupuncture cardiovascular responses. Auton. Neurosci. 118, 43–50.
Uchida, S., Shimura, M., Ohsawa, H., Suzuki, A., 2007. Neural mechanism of bradycardic responses elicited by acupuncture-like stimulation to a hind limb in anesthetized rats. J. Physiol. Sci. 57 (6), 377–382.
Uchida, S., Kagitani, F., Hotta, H., 2008. Mechanism of the reflex inhibition of heart rate elicited by acupuncture-like stimulation in anesthetized rats. Auton. Neurosci. 143, 12–19.
Wessberg, J., Olausson, H., Fernstrom, W.F., Vallbo, B.A., 2003. Receptive field properties of unmyelinated tactile afferents in the human skin. J. Neurophysiol. 89, 1567–1575.
Yamamoto, H., Kawada, T., Kamiya, A., Kita, T., Sugimachi, M., 2008. Electroacupuncture changes the relationship between cardiac and renal sympathetic nerve activities in anesthetized cats. Auton. Neurosci. 144 (1–2), 43–49.

Please cite this article as: Yamamoto, H., et al., Involvement of the mechanoreceptors in the sensory mechanisms of manual and electrical acupuncture, Auton. Neurosci. (2010), doi:10.1016/j.autneu.2010.11.004

Am J Physiol Regul Integr Comp Physiol 300: R155–R165, 2011.
First published November 3, 2010; doi:10.1152/ajpregu.00540.2010.

Dynamic characteristics of baroreflex neural and peripheral arcs are preserved in spontaneously hypertensive rats

Toru Kawada,[1] Shuji Shimizu,[1,2] Atsunori Kamiya,[1] Yusuke Sata,[1] Kazunori Uemura,[1] and Masaru Sugimachi[1]

[1]*Department of Cardiovascular Dynamics, National Cerebral and Cardiovascular Center Research Institute, Osaka, Japan; and* [2]*Japan Association for the Advancement of Medical Equipment, Tokyo, Japan*

Submitted 18 August 2010; accepted in final form 3 November 2010

Kawada T, Shimizu S, Kamiya A, Sata Y, Uemura K, Sugimachi M. Dynamic characteristics of baroreflex neural and peripheral arcs are preserved in spontaneously hypertensive rats. *Am J Physiol Regul Integr Comp Physiol* 300: R155–R165, 2011. First published November 3, 2010; doi:10.1152/ajpregu.00540.2010.—Although baroreceptors are known to reset to operate in a higher pressure range in spontaneously hypertensive rats (SHR), the total profile of dynamic arterial pressure (AP) regulation remains to be clarified. We estimated open-loop transfer functions of the carotid sinus baroreflex in SHR and Wistar Kyoto (WKY) rats. Mean input pressures were set at 120 (WKY_{120} and SHR_{120}) and 160 mmHg (SHR_{160}). The neural arc transfer function from carotid sinus pressure to efferent splanchnic sympathetic nerve activity (SNA) revealed derivative characteristics in both WKY and SHR. The slope of dynamic gain (in decibels per decade) between 0.1 and 1 Hz was not different between WKY_{120} (10.1 ± 1.0) and SHR_{120} (10.4 ± 1.1) but was significantly greater in SHR_{160} (13.2 ± 0.8, $P < 0.05$ with Bonferroni correction) than in SHR_{120}. The peripheral arc transfer function from SNA to AP showed low-pass characteristics. The slope of dynamic gain (in decibels per decade) did not differ between WKY_{120} (−34.0 ± 1.2) and SHR_{120} (−31.4 ± 1.0) or between SHR_{120} and SHR_{160} (−32.8 ± 1.3). The total baroreflex showed low-pass characteristics and the dynamic gain at 0.01 Hz did not differ between WKY_{120} (0.91 ± 0.08) and SHR_{120} (0.84 ± 0.13) or between SHR_{120} and SHR_{160} (0.83 ± 0.11). In both WKY and SHR, the declining slope of dynamic gain was significantly gentler for the total baroreflex than for the peripheral arc, suggesting improved dynamic AP response in the total baroreflex. In conclusion, the dynamic characteristics of AP regulation by the carotid sinus baroreflex were well preserved in SHR despite significantly higher mean AP.

systems analysis; transfer function; white noise; sympathetic nerve activity; arterial pressure

THE ARTERIAL BAROREFLEX IS an important negative feedback system that stabilizes systemic arterial pressure (AP) against exogenous disturbances in daily activities. The sympathetic limb of the arterial baroreflex system may be analyzed by dividing it into two principal subsystems (23). One is a controller subsystem that describes the relationship between baroreceptor pressure input and efferent sympathetic nerve activity (SNA). The other is an effector subsystem that describes the relationship between SNA and AP. Hereafter, in this article, we refer to the former as the neural arc and the latter as the peripheral arc (9). In normal physiological conditions, changes in AP affect SNA via the neural arc, and the changes in SNA, in turn, affect AP via the peripheral arc. This closed-loop operation makes it difficult to identify the dynamic characteristics of the neural and peripheral arcs separately (see APPENDIX) (18). To circumvent the closed-loop problem, the carotid sinus baroreceptor regions were isolated from the systemic circulation, and open-loop transfer function analyses were performed in anesthetized rabbits (9) and rats (31). In both species, the neural arc revealed "derivative" characteristics, which means that the dynamic gain of the SNA response becomes greater as the frequency of modulation increases. In contrast, the peripheral arc showed "low-pass" characteristics, which means that the dynamic gain of the AP response becomes smaller as the frequency of modulation increases. It has been interpreted that the fast neural arc partially compensates for the slow peripheral arc to improve the speed of response of the total baroreflex system (9).

In chronic hypertension, the arterial baroreflex is reset to operate in a higher pressure range (2). Both carotid sinus (24) and aortic baroreceptors (30) show the resetting in spontaneously hypertensive rats (SHR). Although changes in vascular properties induced by sustained hypertension, such as reduced distensibility, may decrease the baroreflex sensitivity, the dynamic characteristics of AP regulation by the arterial baroreflex in hypertension are not fully understood. In a previous study, Harada et al. (7) have shown that the baroreflex neural arc retains its derivative characteristics in SHR. Since they perturbed AP by aortic balloon inflation and deflation, they were unable to quantify the dynamic AP response to changes in SNA (i.e., the peripheral arc). As a result, the total profile of the dynamic AP regulation in SHR remains to be clarified. The aim of the present study was to comprehensively identify the dynamic characteristics of the neural arc, peripheral arc, and total baroreflex in SHR and compare them with those estimated in normotensive Wistar Kyoto rats (WKY).

MATERIALS AND METHODS

Animals were cared for in strict accordance with the Guiding Principles for the Care and Use of Animals in the Field of Physiological Sciences, which has been approved by the Physiological Society of Japan. All experimental protocols were reviewed and approved by the Animal Subjects Committee at the National Cerebral and Cardiovascular Center.

Surgical preparation. Main experiments were performed in age-matched male WKY ($n = 7$, 21.6 ± 3.7 wk) and SHR ($n = 6$, 22.2 ± 4.5 wk). Each rat was anesthetized with an intraperitoneal injection (2 ml/kg) of a mixture of urethane (250 mg/ml) and α-chloralose (40 mg/ml), and mechanically ventilated with oxygen-enriched room air. A venous catheter was inserted into the right femoral vein, and the above anesthetic mixture, diluted 20-fold, was administered continuously (2–3 $ml \cdot kg^{-1} \cdot h^{-1}$). An arterial catheter was inserted into the right femoral artery to measure AP. Heart rate (HR) was obtained

Address for reprint requests and other correspondence: T. Kawada, Dept. of Cardiovascular Dynamics, National Cerebral and Cardiovascular Center Research Institute, 5-7-1 Fujishirodai, Suita, Osaka 565–8565, Japan (e-mail: torukawa@res.ncvc.go.jp).

0363-6119/11 Copyright © 2011 the American Physiological Society

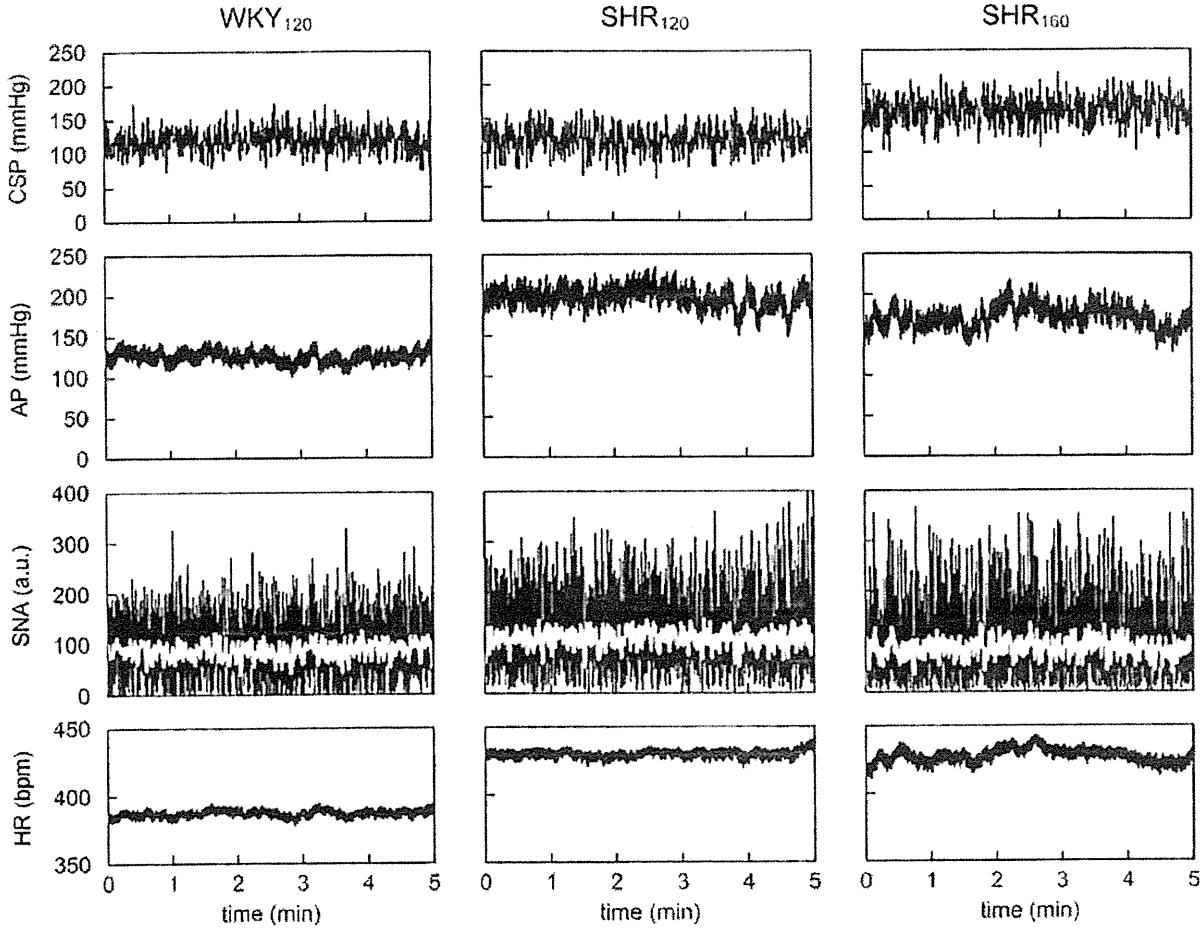

Fig. 1. Typical recordings of carotid sinus pressure (CSP), arterial pressure (AP), sympathetic nerve activity (SNA), and heart rate (HR) obtained from a Wistar Kyoto (WKY) rat and a spontaneously hypertensive rat (SHR). CSP was perturbed according to a Gaussian white noise with mean input pressure of 120 mmHg (WKY_{120} and SHR_{120}) or 160 mmHg (SHR_{160}). White lines in the SNA data indicate 2-s moving average SNA signals.

from AP through a cardiotachometer. Another venous catheter was inserted into the left femoral vein to infuse Ringer solution (6 $ml \cdot kg^{-1} \cdot h^{-1}$).

A postganglionic branch from the splanchnic sympathetic nerve was exposed through a left flank incision and a pair of stainless-steel wire electrodes (Bioflex wire AS633; Cooner Wire, Chatsworth, CA) was attached to record SNA. The nerve and electrodes were covered with silicone glue (Kwik-Sil; World Precision Instruments, Sarasota, FL, USA) for insulation and fixation. To quantify the nerve activity, the preamplified nerve signal was band-pass filtered at 150–1,000 Hz, and then full-wave rectified and low-pass filtered with a cut-off frequency of 30 Hz. Pancuronium bromide ($0.4\ mg \cdot kg^{-1} \cdot h^{-1}$) was administered to prevent muscular activity from contaminating the SNA recording. At the end of the experiment, we confirmed the disappearance of SNA after an intravenous bolus injection of a ganglionic blocker hexamethonium bromide (60 mg/kg) and recorded the noise level.

Table 1. *Mean arterial pressure, heart rate, and sympathetic nerve activity during dynamic input protocol*

	WKY_{120}	SHR_{120}	SHR_{160}
Mean AP, mmHg	105 ± 5	176 ± 17**	143 ± 14†
Mean HR, bpm	406 ± 18	432 ± 19	423 ± 15
Mean SNA, au	85 ± 12	147 ± 15*	110 ± 15†

Data are presented in means ± SE values [$n = 7$ for Wistar-Kyoto (WKY) and $n = 6$ for spontaneously hypertensive rats (SHR)]. AP, arterial pressure; HR, heart rate; SNA, sympathetic nerve activity; bpm, beats per minute; au, arbitrary unit. *$P < 0.05$ and **$P < 0.01$, WKY_{120} vs. SHR_{120} by unpaired-t-test with Bonferroni correction. †$P < 0.05$, SHR_{120} vs. SHR_{160} by paired-t-test with Bonferroni correction.

Bilateral vagal and aortic depressor nerves were sectioned at the neck to avoid reflexes from the cardiopulmonary region and aortic arch. The carotid sinus regions were isolated from the systemic circulation using previously reported procedures (32, 34) with modifications. Briefly, a 7–0 polypropylene suture with a fine needle (PROLENE; Ethicon, Cornelia, GA) was passed through the tissue between the external and internal carotid arteries, and the external carotid artery was ligated close to the carotid bifurcation. The internal carotid artery was embolized by injecting two to three steel balls (0.8 mm in diameter; Tsubaki Nakashima, Nara, Japan) from the common carotid artery. The isolated carotid sinuses were filled with warmed Ringer solution through catheters inserted into the common carotid arteries. The carotid sinus pressure (CSP) was controlled using a servo-controlled piston pump. Heparin sodium (100 U/kg) was given intravenously to prevent blood coagulation. Body temperature was maintained at ~38°C with a heating pad.

Protocols. Some animals showed deterioration of baroreflex responses soon after the completion of the surgical preparation, possibly due to the surgical damage to the carotid sinus nerves or the low brain

perfusion after bilateral common carotid occlusion. The baroreflex study described below was conducted only in animals showing persistent baroreflex-mediated SNA, AP, and HR responses for more than 30 min after completion of the surgical preparation.

To estimate dynamic characteristics of the carotid sinus baroreflex, CSP was perturbed for 20 min using a Gaussian white noise (GWN) signal with a standard deviation of 20 mmHg (11, 12). The whiteness of the input is essential to estimate the system characteristics stably over a frequency range of interest (see APPENDIX). The mean input CSP was set at 120 mmHg in WKY (WKY_{120}) and SHR (SHR_{120}). Taking into account a priori knowledge that the baroreceptor is reset to a higher pressure range in SHR (2, 24), the same rats in SHR_{120} were also tested at a mean input CSP of 160 mmHg (SHR_{160}). The switching interval of GWN was 500 ms. The resulting input power spectral density was relatively constant up to 1 Hz, which was expected to cover the upper frequency range of interest with respect to the sympathetic arterial baroreflex in rats (31).

A supplemental protocol was performed in an additional three 18-wk-old male WKY rats to test the effect of changing the mean input CSP on the transfer function estimation. The GWN input was applied with the mean CSP set at 120 mmHg ($WKY_{120\text{-}S}$) and 160 mmHg ($WKY_{160\text{-}S}$). Six data sets were analyzed by acquiring two data sets from each rat using GWN signals of different sequences.

Data analysis. Data were sampled at 200 Hz using a 16-bit analog-to-digital converter and stored in a dedicated laboratory computer system. Dynamic characteristics of the baroreflex neural arc, peripheral arc, total baroreflex, and HR control were estimated by a standard open-loop transfer function analysis (see APPENDIX) (20). Data analysis was started from 120 s after initiation of the GWN input. The input-output data pairs were resampled at 10 Hz, and 12 segments were processed using 50%-overlapping bins of 1,024 points each.

To facilitate understanding of the transfer function, the step response corresponding to the transfer function was calculated as follows. A system impulse response was derived from the inverse Fourier transform of the transfer function. The step response was then obtained from the time integral of the impulse response.

Because the magnitude of SNA varied among animals depending on the recording conditions, SNA was normalized in each animal by assigning unity to the mean dynamic gain for frequencies below 0.03 Hz in the neural arc transfer function, for WKY_{120} and SHR_{120}. The following parameters of the transfer functions were compared: dynamic gain values at 0.01, 0.1, and 1 Hz ($G_{0.01}$, $G_{0.1}$, and G_1), and the slope of dynamic gain (G_{slope}) for the frequency range of 0.1 to 1 Hz. G_{slope} was calculated by a regression analysis between log frequency and log dynamic gain. For step response analysis of the neural arc, the negative peak response (S_{peak}), time to the negative peak (T_{peak}), and step response at 10 s (S_{10}) were calculated. For step response analyses of the peripheral arc, total baroreflex, and HR control, the steady-state response at 50 s (S_{50}) and initial slope (S_{slope}) were calculated. To calculate S_{slope}, a threshold value was determined at 5% S_{50}, and the

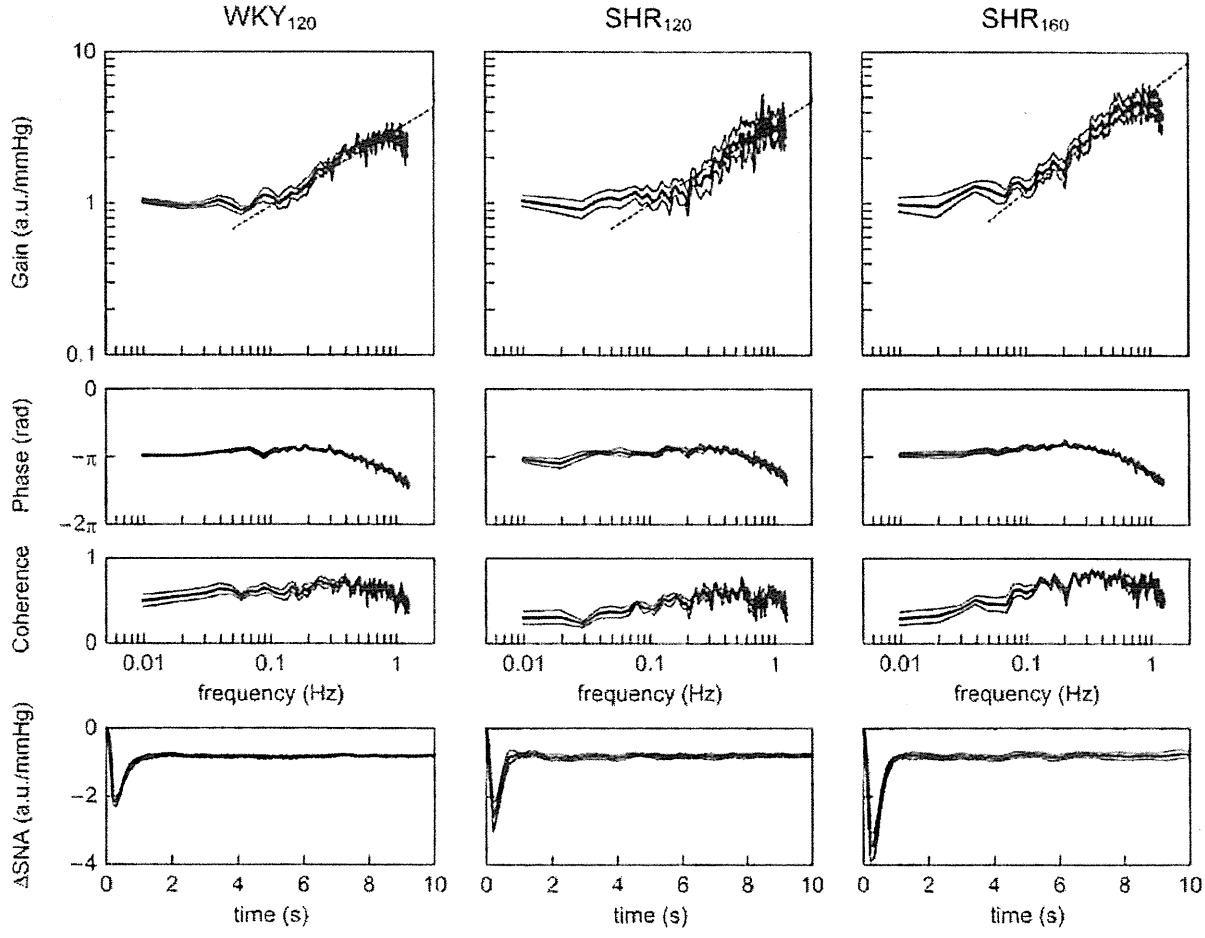

Fig. 2. Transfer functions of the baroreflex neural arc from CSP to SNA averaged for WKY_{120}, SHR_{120}, and SHR_{160} groups. Gain, phase, and coherence plots are shown. In the gain plots, the dashed oblique line indicates the mean slope of the dynamic gain (G_{slope}) estimated in the frequency range from 0.1 to 1 Hz. G_{slope} is significantly steeper in SHR_{160} than in SHR_{120}. *Bottom*: step responses of SNA calculated from the corresponding neural arc transfer functions. The peak response (S_{peak}) is significantly more negative in SHR_{160} than in SHR_{120}. In all panels, the bold and thin lines indicate mean and mean ± SE values, respectively.

first data point that exceeded the threshold was obtained. Starting from this first data point, a regression analysis was repeated while increasing the number of data points for the regression. The steepest slope thus obtained was defined as S_{slope}.

Statistical analysis. All data are presented as means ± SE. Differences between WKY_{120} and SHR_{120} were tested using unpaired *t*-test. Differences between SHR_{120} and SHR_{160} were tested using paired *t*-test. Taking into account the duplicated comparisons of the SHR_{120} data, differences between groups were considered to be significant when $P < 0.05$ with Bonferroni correction (i.e., $P < 0.025$ and $P < 0.005$ were interpreted as $P < 0.05$ and $P < 0.01$, respectively) (5). In the supplemental protocol, parameters were compared between $WKY_{120\text{-}S}$ and $WKY_{160\text{-}S}$ using paired *t*-test.

RESULTS

Figure 1 shows the typical experimental data obtained from an individual rat in the WKY_{120}, SHR_{120}, and SHR_{160} groups. The SHR_{120} and SHR_{160} data were derived from the same animal. In each group, CSP was perturbed according to a GWN signal, which caused variations in AP, SNA, and HR. The mean AP was significantly higher in SHR_{120} than in WKY_{120}, confirming hypertension in SHR (Table 1). The mean AP was significantly lower in SHR_{160} than in SHR_{120}, indicating that increasing the mean CSP enabled the reduction of the mean AP in SHR. The white lines in the SNA plots indicate 2-s moving average signals. Although mean SNA was higher in SHR_{120} than in WKY_{120}, this comparison could be influenced by the normalization of SNA. The mean SNA in SHR_{160} decreased significantly to 74 ± 6% of that in SHR_{120}. Although changes in mean HR appeared to parallel the changes in mean AP, there were no significant changes across the groups (Table 1).

The neural arc transfer functions averaged from the WKY_{120}, SHR_{120}, and SHR_{160} groups are shown in Fig. 2. In the gain plots, $G_{0.01}$ approximated unity in WKY_{120} and SHR_{120} because of the normalization procedure (Table 2). The dynamic gain became greater as the frequency increased above 0.1 Hz. There were no significant differences in $G_{0.1}$, G_1, and G_{slope} between WKY_{120} and SHR_{120}. $G_{0.01}$ also approximated unity in SHR_{160}, although SNA was normalized by the same normalization factor used for the SHR_{120} data. While $G_{0.1}$ did not differ significantly between SHR_{120} and SHR_{160}, G_1 and G_{slope} were significantly greater in SHR_{160}. The phase plots of three groups were similar: the phase was close to $-\pi$ radians at 0.01 Hz, deviated slightly toward 0 radians until 0.5 Hz, and then delayed beyond $-\pi$ radians as the frequency increased above 0.7 Hz. For the step responses, S_{10} and T_{peak} did not differ between WKY_{120} and SHR_{120} or between SHR_{120} and SHR_{160}. S_{peak} was not significantly different between WKY_{120} and SHR_{120} but was significantly more negative in SHR_{160} than in SHR_{120}.

The peripheral arc transfer functions averaged from the WKY_{120}, SHR_{120}, and SHR_{160} groups are shown in Fig. 3. In the gain plots, the dynamic gain became smaller, as the frequency increased above 0.05 Hz. $G_{0.01}$, $G_{0.1}$, G_1, and G_{slope} did not differ significantly between WKY_{120} and SHR_{120} or between SHR_{120} and SHR_{160} (Table 2). The phase plots of three groups were similar: the phase approached 0 radians at 0.01 Hz and was delayed by -2π radians as the frequency increased to 1 Hz. For the step responses, S_{50} and S_{slope} did not differ between WKY_{120} and SHR_{120} or between SHR_{120} and SHR_{160}.

Table 2. *Parameters of estimated transfer functions and step responses*

	WKY_{120}	SHR_{120}	SHR_{160}
Neural arc			
$G_{0.01}$, au/mmHg	1.04 ± 0.04	1.06 ± 0.08	1.01 ± 0.11
$G_{0.1}$, au/mmHg	1.15 ± 0.11	1.16 ± 0.14	1.35 ± 0.13
G_1, au/mmHg	2.73 ± 0.21	3.41 ± 0.51	4.84 ± 0.64††
G_{slope}, dB/decade	10.1 ± 1.0	10.4 ± 1.1	13.2 ± 0.8†
S_{10}, au/mmHg	−0.81 ± 0.03	−0.79 ± 0.05	−0.79 ± 0.11
S_{peak}, au/mmHg	−2.22 ± 0.15	−2.71 ± 0.35	−3.60 ± 0.40††
T_{peak}, s	0.37 ± 0.03	0.33 ± 0.02	0.35 ± 0.02
Peripheral arc			
$G_{0.01}$, mmHg/au	0.75 ± 0.07	0.79 ± 0.14	0.79 ± 0.14
$G_{0.1}$, mmHg/au	0.35 ± 0.05	0.48 ± 0.14	0.45 ± 0.12
G_1, mmHg/au	0.014 ± 0.008	0.008 ± 0.002	0.008 ± 0.003
G_{slope}, dB/decade	−34.0 ± 1.2	−31.4 ± 1.0	−32.8 ± 1.3
S_{50}, mmHg/au	0.89 ± 0.06	0.85 ± 0.15	0.81 ± 0.15
S_{slope}, mmHg·au^{-1}·s^{-1}	0.14 ± 0.01	0.20 ± 0.05	0.18 ± 0.05
Total baroreflex			
$G_{0.01}$, mmHg/mmHg	0.91 ± 0.08	0.84 ± 0.13	0.83 ± 0.11
$G_{0.1}$, mmHg/mmHg	0.41 ± 0.06	0.53 ± 0.09	0.58 ± 0.10
G_1, mmHg/mmHg	0.023 ± 0.009	0.025 ± 0.005	0.034 ± 0.006
G_{slope}, dB/decade	−24.6 ± 1.3‡‡	−22.3 ± 1.3‡‡	−19.8 ± 1.3‡‡
S_{50}, mmHg/mmHg	−1.03 ± 0.10	−0.85 ± 0.08	−0.83 ± 0.08
S_{slope}, mmHg·mmHg^{-1}·s^{-1}	−0.20 ± 0.02	−0.28 ± 0.04	−0.32 ± 0.05
HR control			
$G_{0.01}$, bpm/mmHg	0.46 ± 0.05	0.22 ± 0.04**	0.27 ± 0.05
$G_{0.1}$, bpm/mmHg	0.11 ± 0.01	0.04 ± 0.01**	0.08 ± 0.02†
S_{50}, bpm/mmHg	−0.52 ± 0.07	−0.18 ± 0.04**	−0.23 ± 0.05
S_{slope}, bpm·mmHg^{-1}·s^{-1}	−0.050 ± 0.004	−0.025 ± 0.005**	−0.036 ± 0.009

Data are presented as means ± SE ($n = 7$ for WKY and $n = 6$ for SHR). $G_{0.01}$, $G_{0.1}$, and G_1, dynamic gain values at 0.01, 0.1, and 1 Hz, respectively; G_{slope}, slope of dynamic gain between 0.1 and 1 Hz; S_{50}, steady-state response at 50 s; S_{peak}, peak response; S_{slope}, initial slope; S_{10}, step response at 10 s; T_{peak}, time to the negative peak. **$P < 0.01$ WKY_{120} vs. SHR_{120} by unpaired-*t*-test with Bonferroni correction. ††$P < 0.01$ and †$P < 0.05$, SHR_{120} versus SHR_{160} by paired-*t*-test with Bonferroni correction. ‡‡$P < 0.01$, peripheral arc versus total baroreflex by paired-*t*-test in each group.

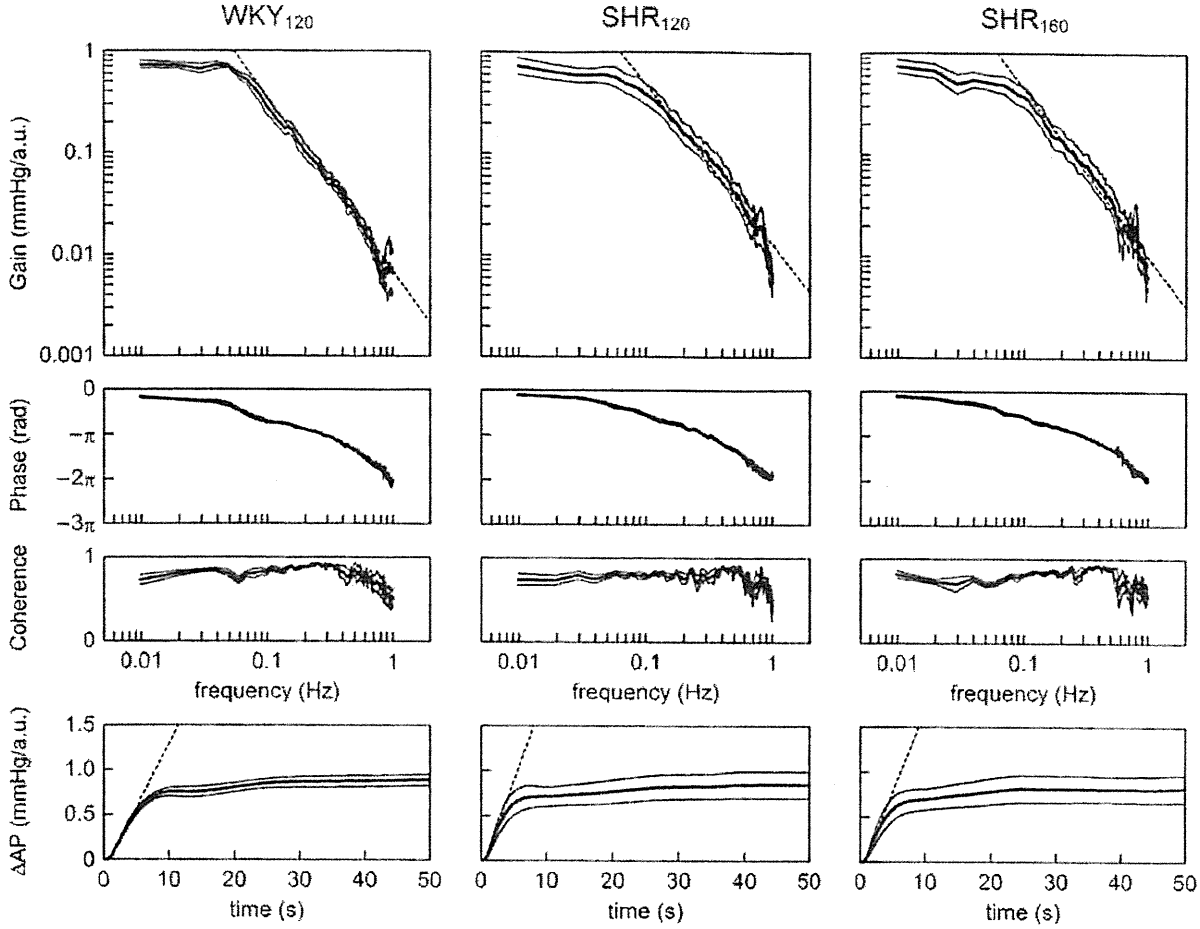

Fig. 3. Transfer functions of the baroreflex peripheral arc from SNA to AP averaged for WKY_{120}, SHR_{120} and SHR_{160} groups. Gain, phase, and coherence plots are shown. The dashed oblique line in the gain plot indicates G_{slope}. There is no significant difference in G_{slope} between WKY_{120} and SHR_{120} or between SHR_{120} and SHR_{160}. *Bottom*: step responses of AP calculated from the corresponding peripheral arc transfer functions. The dashed oblique line in the step response indicates the initial slope (S_{slope}) of the step response. There were no significant differences in S_{slope}. In all panels, the bold and thin lines indicate mean and mean ± SE values, respectively.

The total baroreflex transfer functions are depicted in Fig. 4. In the gain plots, the dynamic gain declined as the frequency increased above 0.05 Hz, indicating low-pass characteristics of the AP response to the CSP input. $G_{0.01}$, $G_{0.1}$, G_1, and G_{slope} did not differ significantly between WKY_{120} and SHR_{120} or between SHR_{120} and SHR_{160} (Table 2). The phase plots of three groups were also similar: the phase approached $-\pi$ radians at 0.01 Hz, reflecting the negative feedback operation attained by the total baroreflex. The phase was delayed as the frequency increased. For the step response, S_{50} and S_{slope} did not differ between WKY_{120} and SHR_{120} or between SHR_{120} and SHR_{160}. Within-group comparisons using paired *t*-test indicated that G_{slope} was significantly less negative in the total baroreflex than in the peripheral arc transfer function (Table 2).

The transfer functions from CSP to HR are shown in Fig. 5. In the gain plots, the dynamic gain decreased as the frequency increased. $G_{0.01}$ and $G_{0.1}$ were significantly smaller in SHR_{120} than in WKY_{120} (Table 2). Although $G_{0.01}$ did not differ between SHR_{120} and SHR_{160}, $G_{0.1}$ was significantly greater in SHR_{160} than in SHR_{120}. G_1 was not compared because coherence near zero and the phase with increased scatter suggested poor reliability of the estimated transfer functions above 0.8 Hz. In the phase plots, the phase approached $-\pi$ radians at 0.01 Hz, indicating that HR responded negatively to the CSP input. For the step responses, both S_{50} and S_{slope} were significantly less negative in SHR_{120} than in WKY_{120}, while S_{50} and S_{slope} did not differ significantly between SHR_{120} and SHR_{160}.

When the carotid sinus baroreflex was virtually closed by adjusting CSP to AP, mean AP (and thus mean CSP) in WKY was close to 120 mmHg and that in SHR was near 160 mmHg (Table 3). The mean HR and SNA in WKY under the baroreflex closed-loop conditions, however, seemed higher than those observed in WKY_{120}. Similarly, the mean HR and SNA in SHR seemed higher than those observed in SHR_{160}.

Data obtained from the supplemental protocol were summarized in Fig. 6 and Table 4. The gray lines indicate transfer functions derived from $WKY_{120\text{-}S}$, while the black lines indicate those derived from $WKY_{160\text{-}S}$. In the neural arc transfer function, dynamic gain values below 0.1 Hz tended to be lower in $WKY_{160\text{-}S}$ than in $WKY_{120\text{-}S}$. G_{slope} did not differ between $WKY_{120\text{-}S}$ and $WKY_{160\text{-}S}$. In the neural arc step response, S_{peak} did not differ significantly, and S_{10} was marginally attenuated in $WKY_{160\text{-}S}$ ($P = 0.06$). In the peripheral arc, parameters of the transfer function did not differ statistically between

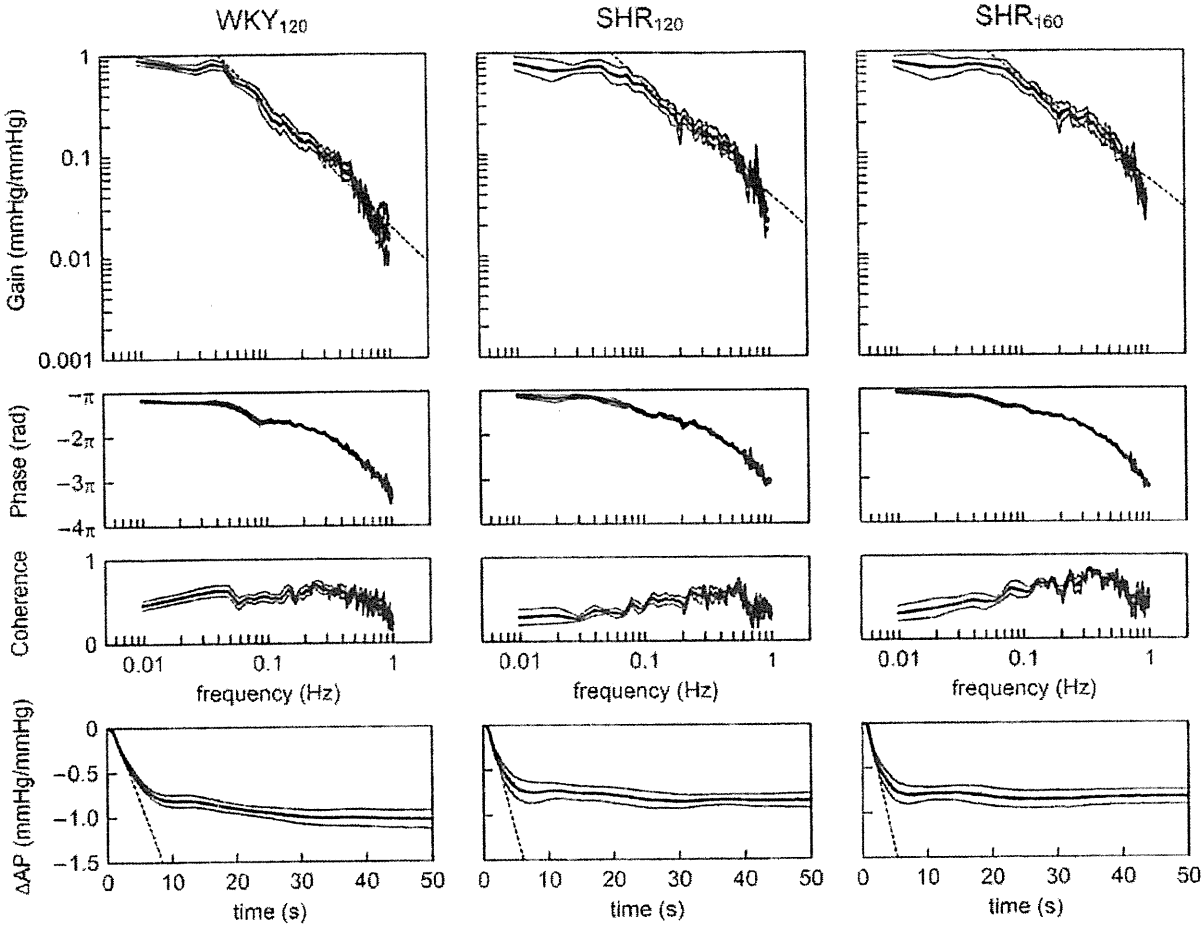

Fig. 4. Transfer functions of the total baroreflex from CSP to AP averaged for WKY_{120}, SHR_{120}, and SHR_{160} groups. Gain, phase, and coherence plots are shown. The dashed oblique line in the gain plot indicates G_{slope}. There is no significant difference in G_{slope} between WKY_{120} and SHR_{120} or between SHR_{120} and SHR_{160}. *Bottom*: step responses of AP calculated from the corresponding total baroreflex transfer functions. The dashed oblique line in the step response indicates the S_{slope}. There were no significant differences in S_{slope}. In all panels, the bold and thin lines indicate mean and mean ± SE values, respectively.

$WKY_{120\text{-}S}$ and $WKY_{160\text{-}S}$. In the peripheral arc step response, S_{slope} was significantly gentler in $WKY_{160\text{-}S}$. In the total baroreflex, although parameters of the transfer function did not differ statistically between $WKY_{120\text{-}S}$ and $WKY_{160\text{-}S}$, parameters of the step response, S_{50} and S_{slope}, were significantly attenuated in $WKY_{160\text{-}S}$.

DISCUSSION

In the present study, we comprehensively identified the open-loop transfer functions of the neural arc, peripheral arc, and total baroreflex in SHR using the normotensive WKY as a reference. Despite significant resetting of the baroreflex, the dynamic characteristics of AP regulation in SHR were comparable to those of WKY, except for a slight augmentation of the derivative characteristics of the neural arc at higher pressure input in SHR. On the other hand, the transfer function related to sympathetic HR control was significantly depressed in SHR compared with WKY.

Neural arc transfer function in SHR. The neural arc transfer function showed derivative characteristics in both WKY and SHR (Fig. 2), consistent with the findings of Harada et al. (7). The present results, however, differ slightly from the previous report in the following aspect. We demonstrated that G_1 and G_{slope} were significantly greater, and S_{peak} was significantly more negative in SHR_{160} than in SHR_{120}, indicating that higher pressure input enhanced the derivative characteristics in SHR. This was not simply an effect of the higher pressure input, because the higher pressure input did not increase G_1, G_{slope}, or S_{peak} in WKY (Fig. 6).

Both mechanosensory transduction at baroreceptors and central processing from baroreceptor afferent nerve activity to efferent SNA contribute to the generation of the derivative characteristics of the neural arc (16). According to a study by Brown et al. (1), the frequency response characteristics of aortic nerve discharge are similar between WKY and SHR in the frequency range of 0.1 to 20 Hz. Although direct comparison is difficult, the present results seem to be in line with their findings. Despite significant resetting in the static characteristics (24), dynamic characteristics of the carotid sinus baroreceptor transduction may not change appreciably in SHR.

Peripheral arc transfer function in SHR. There were no significant differences in the parameters of the peripheral arc transfer function between WKY and SHR (Fig. 3 and Table 2). A major neurotransmitter at the sympathetic nerve

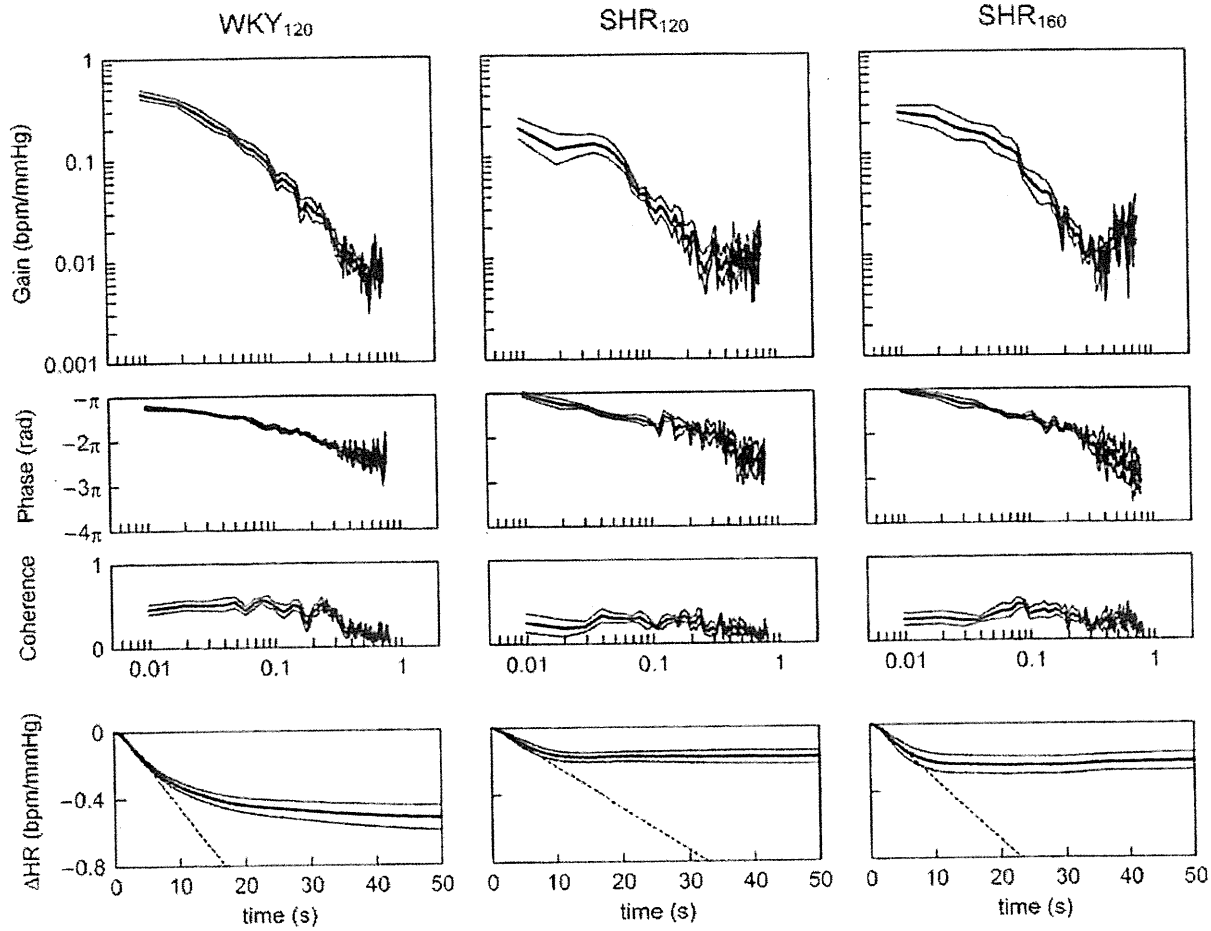

Fig. 5. Transfer functions from CSP to HR averaged for WKY_{120}, SHR_{120}, and SHR_{160} groups. Gain, phase, and coherence plots are shown. The dynamic gain values at 0.01 and 0.1 Hz are significantly smaller in SHR_{120} than in WKY_{120}. *Bottom*: step responses of HR calculated from the corresponding transfer functions. The dashed oblique line in the step response indicates S_{slope}. The steady-state step response and S_{slope} are significantly attenuated in SHR_{120} compared with WKY_{120}. In all panels, the bold and thin lines indicate mean and mean ± SE values, respectively.

endings is norepinephrine. The peripheral arc transfer function may thus reflect the combined dynamic properties of norepinephrine kinetics at the neuroeffector junction and the effector response to adrenergic stimulation (13). Neuronal uptake and α-adrenergic autoinhibition of norepinephrine operate to the same extent during electrical stimulation of the spinal cord in both SHR and WKY (36). Although norepinephrine uptake abnormalities have been reported in SHR (27, 28), the present results indicate that in this model, the influence of altered norepinephrine kinetics on the overall dynamic characteristics of the peripheral arc may be limited.

Table 3. *Mean AP, HR, and SNA under conditions of virtually closed baroreflex*

	WKY	SHR
Mean AP, mmHg	121 ± 3	156 ± 5**
Mean HR, bpm	414 ± 16	433 ± 13
Mean SNA, au	103 ± 14	130 ± 18

Data are presented in means ± SE (n = 7 for WKY and n = 6 for SHR). bpm, beats per minute; au, arbitrary unit. **P < 0.01 by unpaired-t-test.

In pithed rats, pressor response to electrical stimulation of the spinal cord is greater in SHR than in WKY (21, 36). Pressor response to norepinephrine or epinephrine is also enhanced in SHR (36). While the maximum pressor response to methoxamine is greater in SHR than in WKY, the pressor response to submaximal doses of methoxamine is attenuated in SHR (21). The present results suggest that the dynamic characteristics of the peripheral arc are not remarkably different between WKY and SHR despite possible differences in vascular sensitivity to adrenergic stimulation.

Total baroreflex transfer function in SHR. There were no significant differences in the parameters of the total baroreflex transfer function between WKY and SHR (Fig. 4, Table 2), even though AP was significantly higher in SHR than in WKY. In contrast, the step response of the total baroreflex was significantly attenuated in $WKY_{160\text{-}S}$ than in $WKY_{120\text{-}S}$ (Fig. 6, Table 4), indicating that the preservation of the total baroreflex function at the higher pressure input may be unique to SHR. In each of the WKY_{120}, SHR_{120}, and SHR_{160} groups, G_{slope} was significantly less negative in the total baroreflex than in the corresponding peripheral arc, suggesting an improvement of dynamic gain in the higher-frequency range of 0.1 to 1 Hz. The

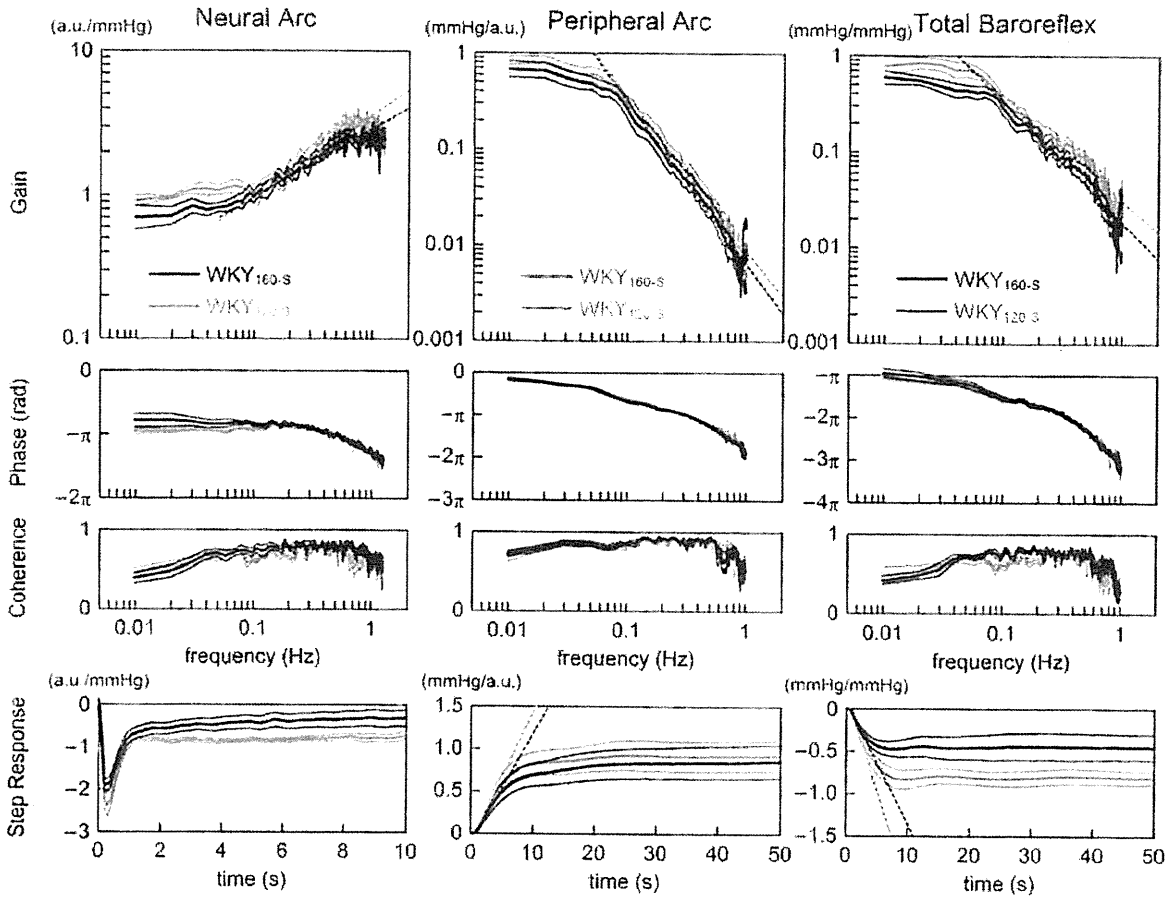

Fig. 6. Transfer functions of the neural arc, peripheral arc, and total baroreflex obtained from an additional protocol. In each panel, the gray lines indicate the transfer functions estimated from $WKY_{120\text{-}S}$. The black lines indicate the transfer functions estimated from $WKY_{160\text{-}S}$. No significant enhancement at the higher pressure input was observed in the derivative characteristics of the neural arc transfer function between 0.1 and 1 Hz. *Bottom*: step responses corresponding to the respective transfer functions. S_{slope} in the peripheral arc was significantly gentler in $WKY_{160\text{-}S}$ than in $WKY_{120\text{-}S}$. Both S_{50} and S_{slope} in the total baroreflex were significantly attenuated in $WKY_{160\text{-}S}$ than in $WKY_{120\text{-}S}$. In all panels, the bold and thin lines indicate mean and mean ± SE values, respectively.

neural arc may thus serve as an accelerating mechanism to improve the dynamic AP regulation in both WKY and SHR. Because G_{slope} in the neural arc was significantly greater in SHR_{160} than in SHR_{120} and G_{slope} in the peripheral arc did not differ between the two groups, G_{slope} in the total loop is expected to be less negative in SHR_{160}. This difference was not detected statistically, however, probably because an increase of G_{slope} by 2.4 dB/decade in the neural arc was partially offset by a decrease of G_{slope} by 1.4 dB/decade in the peripheral arc.

The well-preserved total baroreflex transfer function in SHR is in marked contrast to the significant depression of total baroreflex transfer function in chronic heart failure rats after myocardial infarction (12). Osborn (26) has demonstrated that sinoaortic denervation does not chronically increase mean AP in SHR, suggesting that the arterial baroreflex does not contribute much to the chronic regulation of mean AP in SHR. Nevertheless, the present results imply that the arterial baroreflex in SHR is still important for attenuating acute disturbances in AP.

Transfer function of HR control. In contrast to the total baroreflex transfer function, the transfer function of HR control showed significant depression in dynamic gain in SHR. Although the decreased baroreflex-mediated HR response is primarily attributed to a defect in parasympathetic control (29), the present results obtained in vagotomized rats indicate that the dynamic sympathetic control of HR may also be depressed in SHR. Despite the significant alteration in the sympathetic HR control, the total baroreflex transfer function did not differ between WKY and SHR, suggesting little contribution of HR to the determination of dynamic AP regulation. The lack of significant effect of HR on the dynamic AP regulation is consistent with the findings in rabbits (13, 25).

Baroreflex closed-loop conditions. In the present experimental settings, the baroreflex could be virtually closed by adjusting CSP to AP. The closed-loop operating AP (Table 3) provides a rationale for the selection of the mean input pressure of CSP. When CSP was perturbed around the operating-point pressure, however, mean SNA and AP usually decreased (10). The phenomenon may be related to the input pulsatility and the effect of input amplitude (3, 17, 35). Mean SNA and AP are expected to decrease as the input amplitude of CSP perturbation increases when the mean CSP is lower than the midpoint of the inverse sigmoidal curve characterizing the CSP-SNA relationship.

Table 4. *Parameters of estimated transfer functions and step responses in an additional protocol*

	$WKY_{120\text{-}S}$	$WKY_{160\text{-}S}$
Neural arc		
$G_{0.01}$, au/mmHg	0.93 ± 0.07	0.76 ± 0.14
$G_{0.1}$, au/mmHg	1.08 ± 0.13	1.02 ± 0.09
G_1, au/mmHg	3.12 ± 0.34	2.74 ± 0.25
G_{slope}, dB/decade	11.4 ± 1.2	9.6 ± 0.8
S_{10}, au/mmHg	−0.77 ± 0.09	−0.32 ± 0.19
S_{peak}, au/mmHg	−2.41 ± 0.25	−1.97 ± 0.16
T_{peak}, s	0.35 ± 0.02	0.36 ± 0.03
Peripheral arc		
$G_{0.01}$, mmHg/au	0.83 ± 0.17	0.76 ± 0.17
$G_{0.1}$, mmHg/au	0.35 ± 0.07	0.33 ± 0.08
G_1, mmHg/au	0.025 ± 0.015	0.030 ± 0.017
G_{slope} , dB/decade	−32.1 ± 1.0	−33.7 ± 1.2
S_{50}, mmHg/au	0.92 ± 0.18	0.85 ± 0.20
S_{slope}, mmHg·au^{-1}·s^{-1}	0.15 ± 0.03	0.13 ± 0.03**
Total baroreflex		
$G_{0.01}$, mmHg/mmHg	0.88 ± 0.19	0.63 ± 0.08
$G_{0.1}$, mmHg/mmHg	0.39 ± 0.06	0.35 ± 0.06
G_1, mmHg/mmHg	0.022 ± 0.009	0.042 ± 0.022
G_{slope}, dB/decade	−21.6 ± 0.9	−24.8 ± 1.6
S_{50}, mmHg/mmHg	−0.81 ± 0.08	−0.45 ± 0.15*
S_{slope} , mmHg·mmHg^{-1}·s^{-1}	−0.22 ± 0.03	−0.14 ± 0.04*

Data are presented as means ± SE (n = 6 data sets from 3 rats). *P < 0.05 and **P < 0.01 by paired t-test.

Limitation. First, we performed the experiments in anesthetized rats, which might have affected the estimation of baroreflex function. However, since we compared the baroreflex dynamic characteristics between WKY and SHR under the same anesthetic procedures, the interpretations of the present results may be reasonable. Second, although we examined splanchnic SNA as a representative of systemic SNA, the dynamic characteristics of SNA response could vary in different neural districts (15). Nevertheless, the derivative characteristics of the neural arc in SHR were also evident even when renal SNA was evaluated (7). Third, we occluded the common carotid arteries to isolate the carotid sinuses. Although the vertebral arteries were preserved, we cannot rule out the possibility that the carotid occlusion might have affected the present results. Finally, we transected the vagal nerves to obtain baroreflex open-loop conditions. Further studies are needed to clarify the role of the vagal system in dynamic cardiovascular regulation. Especially, the dynamic HR control may vary greatly in the presence or absence of the vagal efferent nerves (22).

In summary, the neural arc transfer function retained the derivative characteristics in SHR. The peripheral arc and total baroreflex transfer function did not differ significantly between SHR and WKY, suggesting that dynamic AP regulation was well preserved in SHR. In contrast, the dynamic sympathetic HR control seemed significantly attenuated in SHR compared with WKY.

Perspectives and Significance

The arterial baroreflex has been considered to play a minor role in the long-term AP regulation, since denervation of baroreceptor-afferent fibers does not result in a long-lasting hypertension (4, 6). Recent findings, however, indicate that the stimulation of baroreceptor afferent fibers may reduce SNA and AP for a longer period (19). A carotid baroreceptor stimulator has been explored as an alternative therapy for multiple drug-resistant hypertension (8). The device, however, does not seem to take the dynamic characteristics of AP regulation into account and delivers a prescribed stimulation. Ideally, such devices should be activated on a necessary basis, i.e., depressor and pressor function should operate only in the face of hypertensive and hypotensive events, respectively. Understanding of the dynamic characteristics of AP regula-

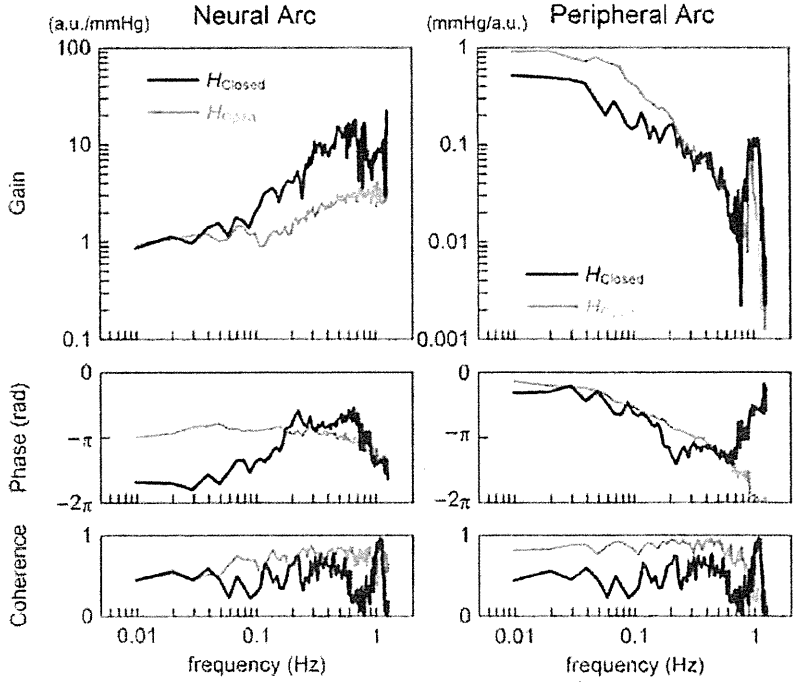

Fig. 7. Comparison of the transfer functions estimated using open-loop data with an exogenous perturbation (gray lines, H_{Open}) and those estimated using closed-loop baseline data without exogenous perturbations (black lines, H_{Closed}) in the same rat. The transfer functions estimated using closed-loop baseline data do not usually extract the dynamic characteristics of the baroreflex neural and peripheral arcs precisely (see APPENDIX for details).

tion in physiological and pathological conditions will contribute to designing an intelligent controller system of such devices (14, 33).

APPENDIX

Consideration on open-loop systems analysis. If a standard transfer function analysis is applied to closed-loop baseline data without exogenous perturbations, the resultant transfer function cannot usually extract open-loop system characteristics precisely. Fig. 7 represents neural and peripheral arc transfer functions estimated using open-loop data with an exogenous CSP input (the gray lines, H_{Open}) and those estimated using closed-loop baseline data without exogenous perturbations (the black lines, H_{Closed}) in the same rat. In the gain plot of the neural arc, although H_{Closed} reveals derivative characteristics, they are much more exaggerated than those seen in H_{Open}. The phase plot of H_{Closed} does not reflect the inverse relation between CSP and SNA below 0.1 Hz. In the gain plot of the peripheral arc, dynamic gain values below 0.2 Hz are smaller in H_{Closed} than in H_{Open}. Although the phase plots are similar between H_{Closed} and H_{Open}, they are dissociated, for instance, at around 0.2 Hz. The phase plots of H_{Closed} are mathematically reversed, and the coherence plots of H_{Closed} are mathematically identical between the neural and peripheral arcs. To what extent H_{Closed} resembles H_{Open} critically depends on the property and magnitude of inherent noise under a given condition, which is usually unknown.

Whiteness of an input signal is prerequisite to estimate a system open-loop transfer function as follows. Take the estimation of a neural arc transfer function, for example. SNA can be expressed in the frequency domain as

$$SNA(f) = H_N(f)CSP(f) + N(f) \quad (A1)$$

where $SNA(f)$, $CSP(f)$, and $N(f)$ denote Fourier transforms of SNA, CSP, and inherent central noise that is unknown. $H_N(f)$ represents the neural arc transfer function. Calculating cross-spectral densities between terms of *Eq. A1* and $CSP(f)$ and performing ensemble averages, we have

$$E[SNA(f)CSP(f)^*] = H_N(f)E[CSP(f)CSP(f)^*] + E[N(f)CSP(f)^*] \quad (A2)$$

where $CSP(f)^*$ indicates a complex conjugate of $CSP(f)$. Because the system characteristics are supposed to be time invariant, $H_N(f)$ can be outside the operation of ensemble average, $E[\ldots]$. The last term $E[N(f)CSP(f)^*]$ asymptotically diminishes when CSP is white noise, because the white noise is statistically independent of other signals. Therefore, $H_N(f)$ can be estimated as follows:

$$H_N(f) = \frac{E[SNA(f)CSP(f)^*]}{E[CSP(f)CSP(f)^*]} \quad (A3)$$

Note that the inherent noise in SNA can affect AP through the baroreflex peripheral arc. Under baroreflex closed-loop conditions, CSP is inevitably influenced by AP and thus by the inherent noise in SNA. In other words, $N(f)$ and $CSP(f)$ are no longer independent once the baroreflex is closed. In this situation, $H_N(f)$ has to be calculated as

$$H_N(f) = \frac{E[SNA(f)CSP(f)^*] - E[N(f)CSP(f)^*]}{E[CSP(f)CSP(f)^*]} \quad (A4)$$

Applying *Eq. A3* instead of *Eq. A4* is one of the reasons for the dissociation between H_{Closed} and H_{Open}. Unfortunately, *Eq. A4* cannot be used ordinarily for analyzing the closed-loop data because $N(f)$ is unknown.

Another important issue is that *Eq. A3* can be ill posed if the denominator is close to zero. In other words, CSP needs to have sufficient power spectral densities at all the frequencies of interest. If there are no sufficient inputs at specific frequencies, there is no way to identify the system characteristics at those frequencies without any assumption or a priori knowledge about the system. The white noise input, which is rich in frequency components, meets the conditions required to stably solve the *Eq. A3*.

GRANTS

This study was supported by Health and Labour Sciences Research Grants (H18-nano-Ippan-003, H19-nano-Ippan-009, H20-katsudo-Shitei-007, and H21-nano-Ippan-005) from the Ministry of Health, Labour and Welfare of Japan; by a Grant-in-Aid for Scientific Research (No. 20390462) from the Ministry of Education, Culture, Sports, Science and Technology of Japan; and by the Industrial Technology Research Grant Program from the New Energy and Industrial Technology Development Organization of Japan.

DISCLOSURES

No conflicts of interest, financial or otherwise, are declared by the authors.

REFERENCES

1. **Brown AM, Saum WR, Yasui S.** Baroreceptor dynamics and their relationship to afferent fiber type and hypertension. *Circ Res* 42: 694–702, 1978.
2. **Chapleau, MW.** Arterial baroreflexes. In: *Hypertension Primer* (4th ed), edited by Izzo JL Jr, Sica DA, and Black HR. Philadelphia, PA: Lippincott Williams & Wilkins, 2008, p. 120–123.
3. **Chapleau MW, Abboud FM.** Contrasting effects of static and pulsatile pressure on carotid baroreceptor activity in dogs. *Circ Res* 61: 648–658, 1987.
4. **Cowley AW Jr, Liard JF, Guyton AC.** Role of baroreceptor reflex in daily control of arterial blood pressure and other variables in dogs. *Circ Res* 32: 564–576, 1973.
5. **Glantz SA.** *Primer of Biostatistics* (5th ed). New York, NY: McGraw-Hill, 2002.
6. **Guyton AC, Coleman TG, Cowley AW Jr, Manning RD Jr, Norman RA Jr, Ferguson JD.** Brief reviews: A systems analysis approach to understanding long-range arterial blood pressure control and hypertension. *Circ Res* 35: 159–176, 1974.
7. **Harada S, Imaizumi T, Ando S, Hirooka Y, Sunagawa K, Takeshita A.** Arterial baroreflex dynamics in normotensive and spontaneously hypertensive rats. *Am J Physiol Regul Integr Comp Physiol* 263: R524–R528, 1992.
8. **Heusser K, Tank J, Engeli S, Diedrich A, Menne J, Eckert S, Peters T, Sweep FC, Haller H, Pichlmaier AM, Luft FC, Jordan J.** Carotid baroreceptor stimulation, sympathetic activity, baroreflex function, and blood pressure in hypertensive patients. *Hypertension* 55: 619–626, 2010.
9. **Ikeda Y, Kawada T, Sugimachi M, Kawaguchi O, Shishido T, Sato T, Miyano H, Matsuura W, Alexander J Jr, Sunagawa K.** Neural arc of baroreflex optimizes dynamic pressure regulation in achieving both stability and quickness. *Am J Physiol Heart Circ Physiol* 271: H882–H890, 1996.
10. **Kashihara K, Takahashi Y, Chatani K, Kawada T, Zheng C, Li M, Sugimachi M, Sunagawa K.** Intravenous angiotensin II does not affect dynamic baroreflex characteristics of the neural or peripheral arc. *Jpn J Physiol* 53: 135–143, 2003.
11. **Kawada T, Kamiya A, Li M, Shimizu S, Uemura K, Yamamoto H, Sugimachi M.** High levels of circulating angiotensin II shift the open-loop baroreflex control of splanchnic sympathetic nerve activity, heart rate and arterial pressure in anesthetized rats. *J Physiol Sci* 59: 447–455, 2009.
12. **Kawada T, Li M, Kamiya A, Shimizu S, Uemura K, Yamamoto H, Sugimachi M.** Open-loop dynamic and static characteristics of the carotid sinus baroreflex in rats with chronic heart failure after myocardial infarction. *J Physiol Sci* 60: 283–298, 2010.
13. **Kawada T, Miyamoto T, Uemura K, Kashihara K, Kamiya A, Sugimachi M, Sunagawa K.** Effects of neuronal norepinephrine uptake blockade on baroreflex neural and peripheral arc transfer characteristics. *Am J Physiol Regul Integr Comp Physiol* 286: R1110–R1120, 2004.
14. **Kawada T, Shimizu S, Yamamoto H, Shishido T, Kamiya A, Miyamoto T, Sunagawa K, Sugimachi M.** Servo-controlled hind-limb electrical stimulation for short-term arterial pressure control. *Circ J* 73: 851–859, 2009.
15. **Kawada T, Shishido T, Inagaki M, Tatewaki T, Zheng C, Yanagiya Y, Sugimachi M, Sunagawa K.** Differential dynamic baroreflex regulation